89-17

Solution of the Hydrodynamic Device Model Using High-Order Non-Oscillatory Shock Capturing Algorithms

by

Emad Fatemi,[†] Joseph Jerome,[††]

and Stanley Osher[†††]

1. INTRODUCTION

A micron $n^+ - n - n^+$ silicon diode is simulated via the hydrodynamic model for carrier transport. The numerical algorithms employed are for the non-steady case, and a limiting process is used to reach steady state. The novelty of our simulation lies in the shock capturing algorithms employed, and indeed shocks, or very rapid transition regimes, are observed in the transient case for the coupled system, consisting of the potential equation and the conservation equations describing charge, momentum, and energy transfer for the electron carriers. These algorithms, termed essentially non-oscillatory, have been successfully applied in other contexts to model the flow in gas dynamics, magnetohydrodynamics and other physical situations involving the conservation laws of fluid mechanics. The method here is first order in time, but the use of small time steps allows for good accuracy. Runge-Kutta methods allow one to achieve higher accuracy in time if desired. The spatial accuracy is of high order in regions of smoothness.

[†]Department of Mathematics, UCLA, Los Angeles, CA 90024. Research supported by NSF grant DMS88-11863.
[††]Department of Mathematics, Northwestern University, Evanston, IL 60208. Research Supported by NSF grant DMS-8721742.
[†††]Department of Mathematics, UCLA, Los Angeles, CA 90024. Research supported by NSF grant DMS88-11863, DARPA grant in the ACMP program, ONR grant N00014-86-K-0691, and NASA Langley grant NAG1-270.

The conservation laws for charge, momentum, and energy for each carrier can be obtained by taking the first three moments of the Boltzmann equation [see Blotekjaer [3], Rudan and Odeh [23], and Cercignani [4]]. This will result in a system of five equations with fourteen variables in three dimensional space. These variables are defined by particle density n, velocity v, internal energy e_I, heat flux q, and symmetric pressure tensor p. In order to close the system, we assume that p and q are defined via (cf. Gardner, Jerome and Rose [9]),

$$p_{ij} = \frac{k_b n T}{m}\delta_{ij} \quad q_i = \frac{-\kappa}{m} n \partial_{x_i} T,$$

where k_b is the Boltzmann constant, m is the mass of one carrier, and T is the carrier temperature assumed to be scalar. The moment system also includes average collision terms, denoted C_n, C_p, and C_w, respectively, which describe the rate of change of mass, momentum and energy. They will account for recombination regeneration processes, electron-electron and electron-lattice collisions, and transfer of energy between electrons and lattice. Their explicit form, for the application considered here, is given by

$$C_n = 0,$$

$$C_p = \frac{-P}{\tau_p} \qquad (P := \text{carrier momentum density})$$

$$C_w = \frac{-(w - \frac{3}{2} n k_b T_0)}{\tau_w} \qquad (w := \text{carrier energy density})$$

Here we use the following empirical relations [see [9]] for relaxation times and the thermoconductivity constant:

$$\tau_p = \frac{m\mu_0 T_0}{eT}, \quad \tau_w = \frac{3\mu_0 k_b T T_0}{2e v_s^2 (T + T_0)} + \frac{\tau_p}{2}, \quad \kappa = \frac{3\mu_0 k_b^2 T_0}{2e},$$

where T_0 is the temperature of the lattice (possibly a function of space), μ_0 is the electron mobility, e the charge of an electron, and v_s is the saturation velocity. We shall discuss the foundations of these relations below. We note here, for consistency, that e_I is proportional to T, and in the following section we shall define P and w, and describe the equations of the hydrodynamic system and the system boundary conditions.

The recent literature, pertaining to the device model simulated here, includes, in addition to [23] and [9], the studies by Baccarani and Wardeman [1], by Odeh, Rudan, and White [19], and by Fischetti and Rudan [8]. In each case, velocity overshoot effects are simulated, which cannot be recovered from the standard drift-diffusion model. As is now widely understood, the effect is strongly dependent on the semiconductor, and is much more pronounced in gallium arsenide than silicon, for example. Since velocity overshoot is related to variations in termperature and electric field, the energy equation in the hydrodynamic model thus allows for the heat flux term q governed by the Wiedemann-Franz law [2], (note that κn is the conductivity in this law) and the coupling to the potential equation is essential in this case. Moreover, the momentum equation plays the role of a refined constitutive current relation. Rather than seeking modifications of the classical current relation by the incorporation of relevant physical effects beyond critical values of parameters such as $\frac{1}{n}\frac{dn}{dx}$ (see [1] for such values and Thornber [30] for a sophisticated discussion of such augmented relations), we find here that current is induced by variable concentration and momentum within the system.

The validity of the assumptions concerning the collision terms C_p and C_w, termed phenomenological approach in [7], has been discussed by Nougier et al. [18], where agreement within 10%, for n type silicon and p type germanium, has been demonstrated, relative to a direct simulation of the Boltzmann equation, for a wide range of electric fields and lattice temperatures. Further assumptions employed in the model, also used in [1], [23], [19], and [9], are the existence of a scalar quantity for the temperature tensor, constructed from the random velocity, and the parabolic representation for the energy, in terms of its kinetic and thermal components. Following Hess and Sah [13], and [1], we have assumed a constant diffusivity coefficient, which is consistent with the assumptions of constant effective mass, and scalar temperature and diffusivity. This has the effect, via the Einstein relation, of describing the electron mobility as an inverse temperature dependent function.

Thus, in this approach, mobility does not directly depend upon velocity. This mobility relation explicitly dictates the expression for the temperature dependent momentum relaxation times expressed above, as well as the choice, exponent $= -1$, in the Wiedemann-Franz law for the thermal conductivity. The temperature dependent energy relaxation time is deduced by using the empirical expression for the mobility, presented by Caughey and Thomas [5], so as to express drift velocity in terms of temperature. The resulting expression is therefore empirical. The steady-state character of both the resulting relaxation time expressions has been emphasized in [1]. Since we simultaneously obtain information for the transient

analysis, the latter results must be interpreted provisionally with respect to τ_p and τ_w.

The earliest theoretical predictions of velocity overshoot appear to be due to Rees [20], for germanium, and to Ruch [22], for silicon and gallium arsenide. Further studies by Shur [26] and Maloney and Frey [16] gave a detailed qualitative understanding of the phenomenon; in particular, it was understood that the physical principle underlying velocity overshoot is the finite time taken before the energy of the carriers reaches equilibrium with the new field, as they traverse a region of rapidly varying electric field. These ideas, and the relation to ballistic transport, have been discussed and critiqued by several authors (see Shur and Eastman [27] and Hess [12]).

Increasing sophistication of the model followed. While [26] and [16] were based upon the quasi-diode, by 1982 Cook and Frey [6] had incorporated many essential features of the hydrodynamic model, coupled to the potential equation, in their simulations. However, they did make the assumptions not made here, of vanishing heat flux and negligible convective energy term. The former assumption, reducing order, substantially alters the mathematical character of the energy equation in addition to its physical implications; these mathematical implications are manifested principally in two or more dimensions, however. Other attempts to incorporate energy and/or transport effects followed, based upon various models. Thus, the foundation for the work of Tang [29] was the spectral method introduced by Stratten [28], where a spherical harmonic expansion of the distribution function leads

to momentum and energy relations similar to those subsequently derived for the hydrodynamic model. Also, McAndrew, Singhal, and Heasell [17] employ a model involving the momentum equation, but not the energy equation.

The models employed in [1], [23], [19], and [9] are virtually the same, with some variations due to mobility-temperature representations, and the joint connection with relaxation times and the Wiedemann-Franz law. The model in this paper is the same as that of [9]. The numerical methods in this paper, however, are quite different from those in previously reported work. Both the parametric regimes and the iterative differencing schemes used in previous work were chiefly keyed to the elliptic or elliptic/parabolic classification of the underlying equations, in other words, to what might loosely be characterized as the subsonic transport regime, where concentrations and velocities would not be expected to experience shock discontinuities. In steady-state, the relevant "soundspeed" is $\sqrt{k_B T/m}$, obtained by linearization of the density-momentum subsystem. If the density-momentum-energy subsystem is linearized, the traditional "soundspeed" of $\sqrt{\frac{5}{3}k_B T/m}$ is obtained, but this involves the parabolic mode associated with the energy equation. The analysis of [9], in fact, shows that a damped Newton method can be justified by energy type estimates in the subsonic case. The shock capturing methods used herein have both the advantage of simulating broad parameter ranges, including transonic and supersonic flow, as well as being readily extendible to two dimensions. Since, as noted by [1], velocity overshoot is maximally exploited when cold carriers are injected at high field, the simulation should have the capability of covering a broad

temperature range, which suggests regions of transonic flow and complex behavior.

2. SYSTEM AND BOUNDARY CONDITIONS

The moment equations are specified, via the summation convention in three dimensions, as

$$\partial_t(n) + \partial_{x_i}(nv_i) = C_n$$

$$\partial_t(nv_j) + \partial_{x_i}(nv_iv_j + p_{ij}) = nF_j + C_{jp} \quad j^{\text{th}} \text{ component}$$

$$\partial_t(n(\frac{1}{2}v^2 + e_I)) + \partial_{x_i}(nv_i(\frac{1}{2}v^2 + e_I) + p_{ij}v_j + q_i) = nF_iv_i + C_w$$

where all of the terms have been defined except the forcing function F due to the electric field.

The Poisson equation for the electrostatic potential, the first of the Maxwell equations, is given in a one carrier, electron system by

$$\epsilon\nabla^2\Phi = e(n - n_D)$$

where n_D is the density of donors. Thus the forcing function F becomes:

$$F = \frac{e}{m}E = \frac{-e}{m}\nabla\Psi,$$

We define $P = mnv$ and $w = mne_I + \frac{mnv^2}{2} = \frac{3}{2}nk_bT + \frac{1}{2}mnv^2$. Let the vector $u = (n, P, w)$ denote, respectively, density, momentum, and energy of electrons. We get the final form of our equations for electrons and electric potential as:

$$\partial_t(n) + \partial_{x_i}(nv_i) = C_n$$

$$\partial_t(P_j) + \partial_{x_i}(P_i v_j + k_b n T) = -enE_j + C_{jp}$$

$$\partial_t(w) + \partial_{x_i}(v_i(w + k_b n T)) = -env_i E_i + C_w + \partial_{x_i}(\kappa n \partial_{x_i} T)$$

$$\epsilon \nabla^2 \Phi = e(n - n_D)$$

We can write the equations in the compact form in (x, y, z) space as:

$$u_t + f_1(u)_x + f_2(u)_y + f_3(u)_x = C(u) + G(u, \Phi) + (0, 0, \nabla(\kappa n \nabla T))$$

$$\epsilon \nabla^2 \Phi = e(n - n_D)$$

In this paper then we concentrate on solving the following system:

(1a) $$\epsilon \Phi_{xx} = e(n - n_D), \quad E = -\Phi_x,$$

(1b) $$n_t + (nv)_x = 0,$$

$$P_t + (Pv + k_b n T)_x = -enE - \frac{P}{\tau_p},$$

$$w_t + (vw + vk_b n T)_x = -envE - \frac{w - \frac{3}{2} n k_b T_0}{\tau_w} + (\kappa n T_x)_x$$

with the following boundary conditions

$$\Phi(0) = \frac{k_b T}{e} ln(\frac{n(0)}{n_i})$$

$$\Phi(1) = \frac{k_b T}{e} ln(\frac{n(1)}{n_i}) + vbias(t)$$

$$u_x(0) = u_x(1) = 0.$$

This is an incompletely parabolic system, very similar to the Navier-Stokes equations of compressible flow. Boundary conditions of this type for that system have been discussed, e.g. in [10].

3. NUMERICAL SCHEME

The numerical scheme is based on the essentially non-oscillatory shock capturing algorithms developed in [11]. We use a sixth order stencil in space and forward Euler in time. Let $u_j^n = u(j\Delta x, n\Delta t) = u(x_j, t_n)$. Also let $D_- u_j^n = \frac{u_j^n - u_{j-1}^n}{\Delta x}$, $D_+ u_j^n = \frac{u_{j+1}^n - u_j^n}{\Delta x}$,and $D_0 u_j^n = \frac{u_{j+1}^n - u_{j-1}^n}{2\Delta x}$.

Then using the above conventions we can write our scheme as:

$$\epsilon D_+ D_- \Phi_j^n = e(n_j^n - n_{D_j}) \tag{2a}$$

$$E_j^n = -D_0 \Phi_j^n \tag{2b}$$

$$u_j^{n+1} = u_j^n - \frac{\Delta t}{\Delta x}(\hat{f}_{j+\frac{1}{2}} - \hat{f}_{j-\frac{1}{2}}) + \Delta t C_j^n + \Delta t G_j^n + \Delta t D_-(n D_+ T) \tag{2c}$$

We calculate the potential from the density and then we calculate the electric field. We calculate the solution in the next time step from the electric field and the "flux" calculated in the previous step.

The "flux" term, $\hat{f}_{j-\frac{1}{2}}^n$, represents the numerical flux flowing into the jth computational cell [see Lax [15]].

The finite difference scheme (2c) is an approximation of (1b) . The system (1b) is a hyperbolic system of conservation laws with a right hand side which consists of a viscosity term in the third equation, a lower order term and a non-local term which comes from solving the elliptic equation for Φ in terms of n and $\bar{n}_0$ [see 9].

It is well known that solutions of a system of hyperbolic conservation laws develop discontinuities after a finite time for general initial data. These discontinuties

then we compare the divided differences and we move the stencil according to

$$\text{if } |f^i(j+\text{ishift})| \geq |f^i(j+\text{ishift}-1)| \qquad \text{then ishift=ishift} - 1$$

We continue in this manner and let m=j+ishift; then the reconstructed polynomial can be written as:

$$R_{j+\frac{1}{2}}(x) = H^0(m) + H^1(m)(x - x_{m-\frac{1}{2}}) + H^2(m)(x - x_{m-\frac{1}{2}})(x - x_{m+\frac{1}{2}}) + \cdots$$

The value of the flux can be calculated by evaluating the first derivative of R(x) at $x_{j+\frac{1}{2}}$.

The above scheme is known to contain nonphysical "expansion shock" solutions occasionally. To remedy this case let us define a critical cell where $f^{'}(u)$ has a zero in the interval $I = [u_j, u_{j+1}]$. These are the only cells that could contain expansion shocks.

In a critical cell we use the following scheme:

Let $\alpha_{j+\frac{1}{2}} = \max_I |f^{'}(u)|$. Then define the following quantities for $j - r + 1 \leq s \leq j + r$ where r is the order of the scheme:

$$f^+(s) = \frac{1}{2}(f(s) + \alpha_{j+\frac{1}{2}} u(s)) \qquad f^-(s) = \frac{1}{2}(f(s) - \alpha_{j+\frac{1}{2}} u(s))$$

We do the reconstruction for f^- using $ishift = 1$ and for f^+ using $ishift = 0$.

The flux can be calculated as a sum of the flux moving to the right and the flux moving to the left.

$$\hat{f}_{j+\frac{1}{2}} = \hat{f}^+_{j+\frac{1}{2}} + \hat{f}^-_{j+\frac{1}{2}}$$

The above scheme can be extended from scalar equations to systems of conservation laws in many ways. We used the following version in our calculations [see [25]].

Let $u_t + f(u)_x = 0$ be the system. Then let $\frac{\partial f}{\partial u}$ represent the Jacobian matrix of the system.

The above system has a complete set of eigenvectors and there is a matrix U such that:

$$U^{-1}\frac{\partial f}{\partial u}U = \Lambda$$

where Λ is a diagonal matrix.

Let $c^2 = \frac{5k_bT}{3m}$ and $b = \frac{2}{3c^2}$ and $B = \frac{v^2}{3c^2}$ and $h = \frac{3}{2}c^2 + \frac{1}{2}v^2$. Here, c is the velocity of sound waves in the electrons and in this connection we define the Mach number of the fluid as $M = \frac{v}{c}$. For our system the above matrices are explicitly:

$$U = \begin{pmatrix} 1 & 1 & 1 \\ m(v-c) & mv & m(v+c) \\ m(-cv+h) & \frac{1}{2}mv^2 & m(cv+h) \end{pmatrix}$$

$$U^{-1} = \begin{pmatrix} \frac{1}{2}(B+\frac{v}{c}) & -\frac{1}{2}(\frac{1}{cm}+\frac{vb}{m}) & \frac{1}{2}(\frac{b}{m}) \\ 1-B & \frac{vb}{m} & \frac{-b}{m} \\ \frac{1}{2}(B-\frac{v}{c}) & \frac{1}{2}(\frac{1}{cm}-\frac{vb}{m}) & \frac{1}{2}(\frac{b}{m}) \end{pmatrix}$$

$$\Lambda = (\lambda_{ij}) = \begin{pmatrix} v-c & 0 & 0 \\ 0 & v & 0 \\ 0 & 0 & v+c \end{pmatrix}$$

In order to do the field by field decomposition of the fluxes we evaluate the U matrix at the Roe average of u_j and u_{j+1} [see [21]].

Let $\bar{u}_{j+\frac{1}{2}} = u^{Roe}(u_j, u_{j+1})$; then we calculate

$$\bar{f}(s) = U^{-1}(\bar{u}_{j+\frac{1}{2}})f(s)$$

This gives us the components of the divided differences of the f in the direction of the fields; then using the algorithm for scalar equations we calculate the flux for each field. We use $a_{j+\frac{1}{2}} = \lambda(\bar{u}_{j+\frac{1}{2}})$ for each field. Then we transform back to the original variables via:

$$\hat{f}_{j+\frac{1}{2}} = U(\bar{u}_{j+\frac{1}{2}})\hat{\bar{f}}_{j+\frac{1}{2}}$$

This scheme will be r-th order accurate in space where r is the order of the reconstructed polynomial $R_{j+\frac{1}{2}}(x)$. To obtain high order accuracy in time, having the ENO property, one may use the Runge-Kutta methods developed in [25]. However, since our primary interest here was in steady state calculations we used only first order forward differencing in time. The resulting scheme would be unstable if the stencils were fixed; the adaptivity stabilizes the linearly unstable method.

4. THERMAL EQUILIBRIUM

If we fix the bias voltage to be zero we expect the system to reach an equilibrium state where the temperature of the electron converges to the lattice temperature and velocity to zero.

Under these assumptions the system will be simplified to

$$k_b T n_x = e n \Phi_x$$

$$\epsilon \Phi_{xx} = e(n - n_D)$$

$$n_x(0) = n_x(1) = 0$$

$$\Phi(0) = \frac{k_b T}{e} ln(\frac{n(0)}{n_i}) \qquad \Phi(1) = \frac{k_b T}{e} ln(\frac{n(1)}{n_i})$$

Note that we get the following relation:

$$n(x) = n_i e^{\frac{e}{k_b T}\Phi(x)}$$

If we let $\Psi(x) = \frac{e}{k_b T}\Phi(x)$ and $\gamma^2 = \frac{\epsilon k_b T}{e^2}$ then the above system is equivalent to the following non-linear boundary value problems:

$$\begin{cases} \gamma^2 \Psi_{xx} - n_i e^{\Psi(x)} = -n_D(x) \\ \Psi_x(0) = \Psi_x(1) = 0 \end{cases}$$

$$\begin{cases} \gamma^2 ln(n(x))_{xx} - n(x) = -n_D(x) \\ n_x(0) = n_x(1) = 0 \end{cases}$$

Rather than solving any of the above we choose the following initial conditions and let the system evolve in time.

$$n(x,0) = n_D(x) \qquad v(x,0) = 0 \qquad T(x,0) = T_0$$

The calculated solution contains the junction and its electric field. Also, the density has to be used as initial condition for the rest of the calculations. The numerical results are presented in the numerical section.

5. PHYSICAL PARAMETERS OF THE DEVICE

The simulated device is a silicon MOSFET channel. The device is an $n^+ - n - n^+$ junction of length one micron.

We use the following doping profile:

$$n_D(x) = 5 \times 10^{17} cm^{-3} \quad if \quad 0 \leq x \leq .25 \quad or \quad .75 \leq x \leq 1$$

$$n_D(x) = 2 \times 10^{15} cm^{-3} \qquad if \quad .35 \leq x \leq .65$$

The two regions are connected by a properly scaled version of the following polynomial:

$$Q(x) = -5x^7 + 21x^5 - 35x^3 + 35x + 16.$$

We also use the following conditions at the boundary:

$$\Phi(0) = \frac{k_b T}{e} ln(\frac{n(0)}{n_i})$$

$$\Phi(1) = \frac{k_b T}{e} ln(\frac{n(1)}{n_i}) + vbias(t)$$

$$n_x(0) = n_x(1) = 0 \qquad p_x(0) = p_x(1) = 0 \qquad w_x(0) = w_x(1) = 0$$

We use the following system of units:

$$Length : 10^{-6} m = 1 micron \qquad Time : 10^{-12} s = 1 pico \quad second$$

$$Mass : 10^{-30} Kg \qquad Potential : Volt \qquad Temperature : Kelvin$$

$$Energy : 10^{-18} J \qquad Charge : 10^{-18} C \qquad Capacitance : 10^{-18} F$$

In the above system of units the constants have the following values:

$$m = 0.26 m_e = .26 \times .9109 \qquad \mu_0 = 0.14 \qquad e = .1602 \qquad v_s = .1$$

$$k_b = .138046 \times 10^{-4} \qquad n_i = .014 \qquad \epsilon = 11.7 \times 8.85418$$

6. NUMERICAL RESULTS

In the first experiment we calculate the density of electrons under zero bias. The result can be used for calculating the junction capacitance and voltage difference

across the junction. Also we use the calculated density as the initial data for the rest of the experiments.

From a numerical point of view this experiment can be used to test the accuracy of the scheme. Since the velocity and current must go to zero, the difference can be used as a measure of error.

In our experiment velocity and current converged to a small oscillatory solution around the zero value. Also we expect the oscillations in the velocity field to create some difficulty for our numerical scheme since it could lead to differencing in the wrong direction.

Indeed, this created spurious oscillations that were eliminated by a small modification in the ENO scheme. We restricted the movement of the stencil such that it would interpolate across oscillations. This can be done in the following fashion. For the sixth order ENO note that the ishift variable takes values between -5 and 1. We simply forced it to be between -4 and 0. This procedure would create small oscillations across shocks, but one can use a modified version to overcome that difficulty. In that version for updating ishift we use:

$$\text{if } |f^i(j+\text{ishift})| \geq |((1+\epsilon)f^i(j+\text{ishift}-1)| \qquad \text{then ishift=ishift} - 1,$$

where ϵ is of order of the truncation error of the scheme and positive or negative depending on the value of ishift. This would make the choice of stencil biased towards the center. In numerical calculations this modification led to a smoother solution with fewer spurious oscillations.

The results from the the experiment are shown in the fig 2-6. In figure 1 the density of donors is shown for reference. As can be seen in figure 2 ,the electrons from both sides expand into the channel. This creates electron waves which settle down approximately in three pico seconds. The junction is formed and the electric field over the junction is created. In figure 4 the steady state of the velocity is shown. The amplitude of the oscillation indicates the size of the error in the rest of the calculations.

In the next set of experiments we apply one volt at time zero and calculate the evolution of the system in time. The system reaches steady state in approximately five pico seconds. In figure 7 the current is shown as a function of time, and in figures 8 and 9 the evolution of electric field and velocity are shown. In figures 10 and 11, for comparison, we duplicate the results obtained by [19], [9].

As an approximation to an I-V curve we apply a bias voltage in form of a "ramp". Then we graph the calculated current versus voltage in figure 12. If the slope of the ramp is small it would be very close to an I-V curve. There is some oscillation in the curve which is due to the jump in the derivative of the bias voltage. If the slope of the ramp is small, it would disappear. In figures 13-17 we show the evolution of the solution as the velocity is increased.

If the temperature of the lattice is raised the sound speed increases and the Mach number becomes small. To test the scheme for small Mach number we set the lattice temperature at 1000K. The evolution of velocity and temperature are shown in the next two graphs.

In the next experiment we set the lattice temperature to 50K. This would reduce the sound speed . The results are given in figures 20-22. We emphasize that we need to modify our choice of stencil to avoid oscillations across steep gradients or shocks.

In the figures 23 and 24 we show just such a situation where the solution develops a very sharp profile. The density and the velocity are shown here. The shock capturing algorithm is designed to handle such situations.

In the next experiment we set our bias voltage to be a square wave and then a sinusoidal wave. The results are shown in figures 25 -29.

In the last experiment we compare the calculated solutions in the steady state using different orders of accuracy in the x variable. From extensive calculations we found out that momentum is the most sensitive variable to error and comparison of momentum would show errors that are not obvious in the other variables.

The calculated results show *spurious* oscillations for low order schemes that (perhaps surprisingly) *decrease* with *increasing* order of accuracy.

7. CONCLUSION

We presented a numerical scheme that is able to solve the Hydrodynamic model efficiently and accurately.

The scheme was first order in time, but it can be extended to high orders of accuracy using the Runge-Kutta methods developed in [25]. Also the high order accuracy in space turned out to be essential at the junctions. The equations allow

very steep gradients including discontinuous solutions, but there was no observation of steady state shocks. However, if a large bias voltage is applied suddenly, shocks form which dissappear in a short time.

There is current work under progress to extend the calculations to holes and also to two spatial dimensions.

FIGURES

Fig 1: density of donors

Fig 2: velocity

zero bias, $Time = 3$, $\frac{\Delta t}{\Delta x} = .2, \Delta x = .01$

Fig 3: temperature

zero bias, $Time = 3$, $\frac{\Delta t}{\Delta x} = .2, \Delta x = .01$

Fig 4: velocity in steady state

zero bias, $Time = 3$, $\frac{\Delta t}{\Delta x} = .2, \Delta x = .01$

Fig 5: $n - n_D$ in steady state

zero bias, $T = 5$, $\frac{\Delta t}{\Delta x} = .2, \Delta x = .01$

Fig 6: electric field in steady state

zero bias, $Time = 3$, $\frac{\Delta t}{\Delta x} = .2, \Delta x = .01$

Fig 7: Current vs. Time

$v(t) = H(t)$, $Time = 5$, $\frac{\Delta t}{\Delta x} = .2, \Delta x = .01$

Fig 8: electric field in time

$v(t) = H(t)$, $Time = 5$, $\frac{\Delta t}{\Delta x} = .2, \Delta x = .01$

Fig 9: velocity in time

$v(t) = H(t),\ Time = 5, \frac{\Delta t}{\Delta x} = .2, \Delta x = .01$

Fig 10: comparison of velocity profile for

bias voltage 1., 1.5, 2.

Fig 11: comparison of temperature profile for

bias voltage 1., 1.5, 2.

Fig 12: Current vs. Voltage

$v(t) = t,\ Time = 20, \frac{\Delta t}{\Delta x} = .1, \Delta x = .01$

Fig 13: Evolution of density

$v(t) = t,\ Time = 20, \frac{\Delta t}{\Delta x} = .1, \Delta x = .01$

Fig 14: Evolution of electric field

$v(t) = t,\ Time = 20, \frac{\Delta t}{\Delta x} = .1, \Delta x = .01$

Fig 15: Evolution of temperature

$v(t) = t,\ Time = 20, \frac{\Delta t}{\Delta x} = .1, \Delta x = .01$

Fig 16: Evolution of velocity

$v(t) = t,\ Time = 20, \frac{\Delta t}{\Delta x} = .1, \Delta x = .01$

Fig 17: Evolution of Mach number

$v(t) = t,\ Time = 20, \frac{\Delta t}{\Delta x} = .1, \Delta x = .01$

Fig 18: Velocity in time

$v(t) = 2H(t),\ Time = 3, \frac{\Delta t}{\Delta x} = .1, \Delta x = .01, T_0 = 1000K$

Fig 19: evolution of temperature

$v(t) = 2H(t),\ Time = 3, \frac{\Delta t}{\Delta x} = .1, \Delta x = .01, T_0 = 1000K$

Fig 20: density in time

$v(t) = H(t),\ Time = 4, \frac{\Delta t}{\Delta x} = .01, \Delta x = .01, T_0 = 50K$

Fig 21: evolution of mach number

$v(t) = H(t),\ Time = 4, \frac{\Delta t}{\Delta x} = .01, \Delta x = .01, T_0 = 50K$

Fig 22: evolution of density

$v(t) = H(t),\ Time = 4, \frac{\Delta t}{\Delta x} = .01, \Delta x = .01, T_0 = 50K$

Fig 23: density in time

$v(t) = 2H(t),\ Time = 1, \frac{\Delta t}{\Delta x} = .01, \Delta x = .01, T_0 = 50K$

Fig 24: density

$v(t) = 2H(t),\ Time = 1, \frac{\Delta t}{\Delta x} = .01, \Delta x = .01, T_0 = 50K$

Fig 25: Current vs. Time

$v(t) = SQW(t),\ Time = 6, \frac{\Delta t}{\Delta x} = .1, \Delta x = .01, T_0 = 300K$

Fig 26: velocity in Time

$v(t) = SQW(t),\ Time = 6, \frac{\Delta t}{\Delta x} = .1, \Delta x = .01, T_0 = 300K$

Fig 27: Current vs. Time

$v(t) = 2sin(2\pi t),\ Time = 6, \frac{\Delta t}{\Delta x} = .1, \Delta x = .01, T_0 = 300K$

Fig 28: density in time

$v(t) = 2sin(2\pi t),\ Time = 5, \frac{\Delta t}{\Delta x} = .1, \Delta x = .01, T_0 = 300K$

Fig 29: temperature in time

$v(t) = 2sin(2\pi t),\ Time = 5, \frac{\Delta t}{\Delta x} = .1, \Delta x = .01, T_0 = 300K$

Fig 30: density, velocity, and momentum not to scale, third order stencil

Fig 31: density, velocity, and momentum not to scale, sixth order stencil

Acknowledgement: The authors would like to thank Dr. Luis Reyna for his

constructive comments on a first draft of this paper.

REFERENCES

[1] G. Baccarani and M.R. Wordeman, "An investigation of steady-state velocity overshoot effects in Si and GaAs devices", Solid State Electr. **28** (1985), 407-416.

[2] F.J. Blatt, "Physics of electric conduction in solids", McGraw-Hill, New York (1968).

[3] K. Blotekjaer, "Transport equations for electrons in two-valley semiconductors", IEEE Trans. Electron Devices ED-17 (1970), 38-47.

[4] C. Cercignani, "The Boltzmann equation and its application", Springer-Verlag, 1988.

[5] D.M. Caughey and R.E. Thomas, "Carrier mobilities in silicon empirically related to doping and field", Proc. IEEE **55** (1967), 2192-2193.

[6] R.K. Cook and J. Frey, "Two-dimensional numerical simulation of energy transport effects in Si and GaAs", MESFET's, IEEE Trans Electron Devices ED-29 (1982), 970-977.

[7] R.K. Cook and J. Frey, "An effecient technique for two-dimensional simulation of velocity overshoot effects in Si and GaAs devices", COMPEL **1** (1982), 65-87.

[8] M. Fischettei and M. Rudan, "Hydrodynamic and Monte-Carlo simulation of an $n^+ - n - n^+$ device", to appear.

[9] C.L. Gardner, J.W. Jerome, and D.J. Rose, "Numerical methods for the hydrodynamic device model: subsonic flow", IEEE Trans. Computer-Aided Design of Integrated Circuits and Systems, V. 8 (1989), 501-507.

[10] B. Gustafsson and A. Sundstrom, "Incompletely parabolic systems in fluid dynamics", SIAM J. Appl. Math., V. 35, (1978), 343-357.

[11] A. Harten, B. Engquist, S. Osher and S. Chakravarthy, "Uniformly high order accurate essentially non-oscillatory schemes, III", J. Comput. Phys., V. 49 (1987), pp.231-303.

[12] K. Hess, "Ballistic electron transport in semiconductors", IEEE Trans Electron Devices ED-28 (1981), 937-940.

[13] K. Hess and C.T. Sah, "Hot electrons in short-gate charge-coupled devices", IEEE Trans. Electron Devices, ED-25 (1978), 1399-1405.

[14] S. Laux and R. Byrnes, "Semiconductor device simulators using generalized

mobility models", IBM J. Res. Dev. **29** (1985), 289-301.

[15] P.D. Lax and B. Wendroff, "Systems of conservation laws", Comm. Pure Appl. Math, V. 13, (1960), pp. 217-237.

[16] T.J. Maloney and J. Frey, "Transient and steady-state electron transport in GaAs and InP", J. Appl. Phys. **48** (1977), 781-787.

[17] C.C. McAndrew, K. Singhal and E.L. Heasell, "A consistent nonisothermal extension of the Scharfetter-Gummel stable difference approximation", IEEE Electron Dev. Lett. EDL-6 (1985), 446-447.

[18] J.P. Nougier, J. Vaissiere, D. Gasquet, J. Zimmermann, and E. Constant, "Determination of the transient regime in semiconductor devices using relaxation time approximations", J. Appl. Phys. **52** (1981), pp. 825-832.

[19] F. Odeh, M. Rudan and J. White, "Numerical solution of the hydrodynamic model for a one-dimensional semiconductor device", COMPEL 6 (1987), 151-170.

[20] H.D. Rees, "Calculation of distribution functions by exploiting the stability of the steady-state", J. Phys. Chem. Sol. **30** (1967), pp. 643-655.

[21] P. Roe, "Approximate Riemann solvers, parameter vectors, and difference schemes", J. Comput. Phys., V. 43, (1981), pp. 357-372.

[22] J. Ruch, "Electron dynamics in short channel field effect transistors", IEEE Trans. Electron Devices ED-19 (1972), pp. 652-654.

[23] M. Rudan and F. Odeh, "Multi-dimensional discretization scheme for the hydrodynamic model of semiconductor devices", COMPEL **5** (1986), 149-183.

[24] S. Selberherr, "An analysis and simulation of semiconductor devices", Springer-Verlag, 1984.

[25] C.-W. Shu and S. Osher, "Efficient implementation of essentially non-oscillatory shock capturing schemes, II, "J. Comp. Physics, (1989), to appear.

[26] M.S. Shur, "Influence of nonuniform field distribution on frequency limits of GaAs field effect transistors", Elect. Lett. **12** (1976), pp. 615-616.

[27] M.S. Shur and E.F. Eastman, "Ballistic transport in semiconductors at low temperatures for low-power high-speed logic", IEEE Trans. Electron Devices ED-26 (1979), pp. 1677-1683.

[28] R. Stratten, "Diffusion of hot and cold electrons in semiconductor barriers",

Phys. Rev. **126** (1962), pp. 2002-2014.

[29] T. Tang, "Extension of the Scharfetter-Gummel algorithm to the energy balance equation", IEEE Trans. Electron Devices ED-31 (1984), pp. 1912-1914.

[30] K.K. Thornber, "Current equations for velocity overshoot", IEEE Electron Dev. Lett. EDL-3 (1982), pp. 69-71.

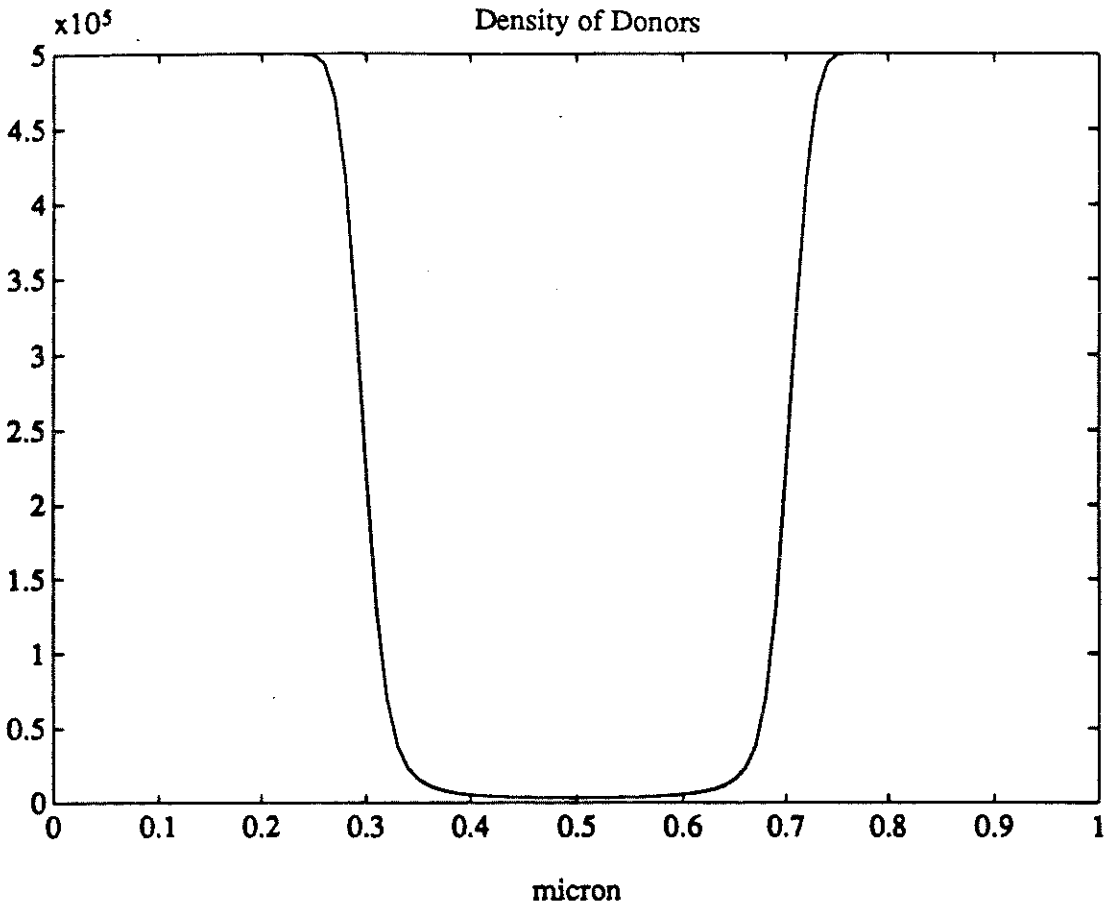

Fig 1: density of donors

Time= 3 Bias Voltage = 0

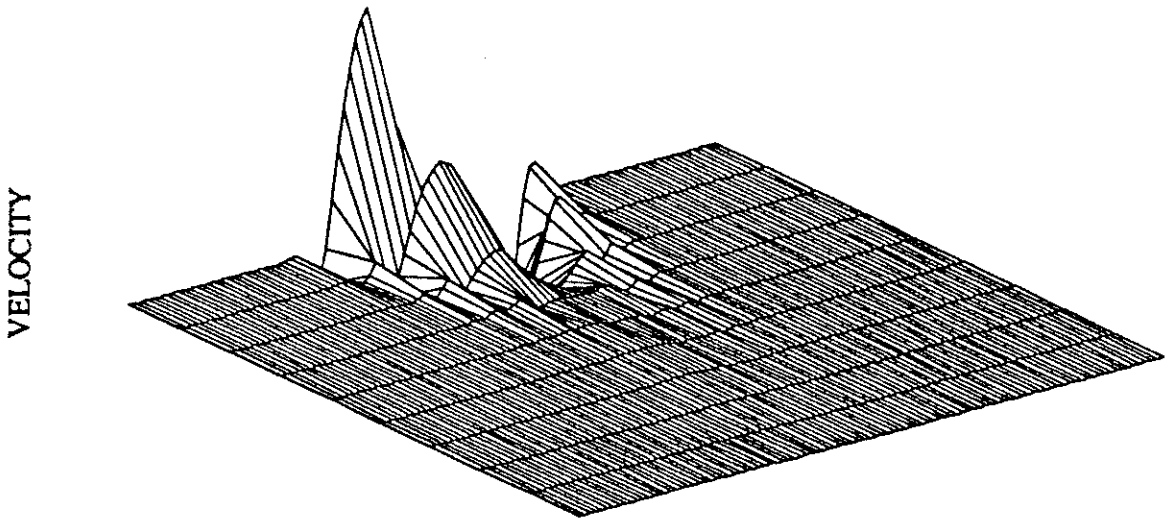

Fig 2: velocity

zero bias, $Time = 3$, $\frac{\Delta t}{\Delta x} = .2, \Delta x = .01$

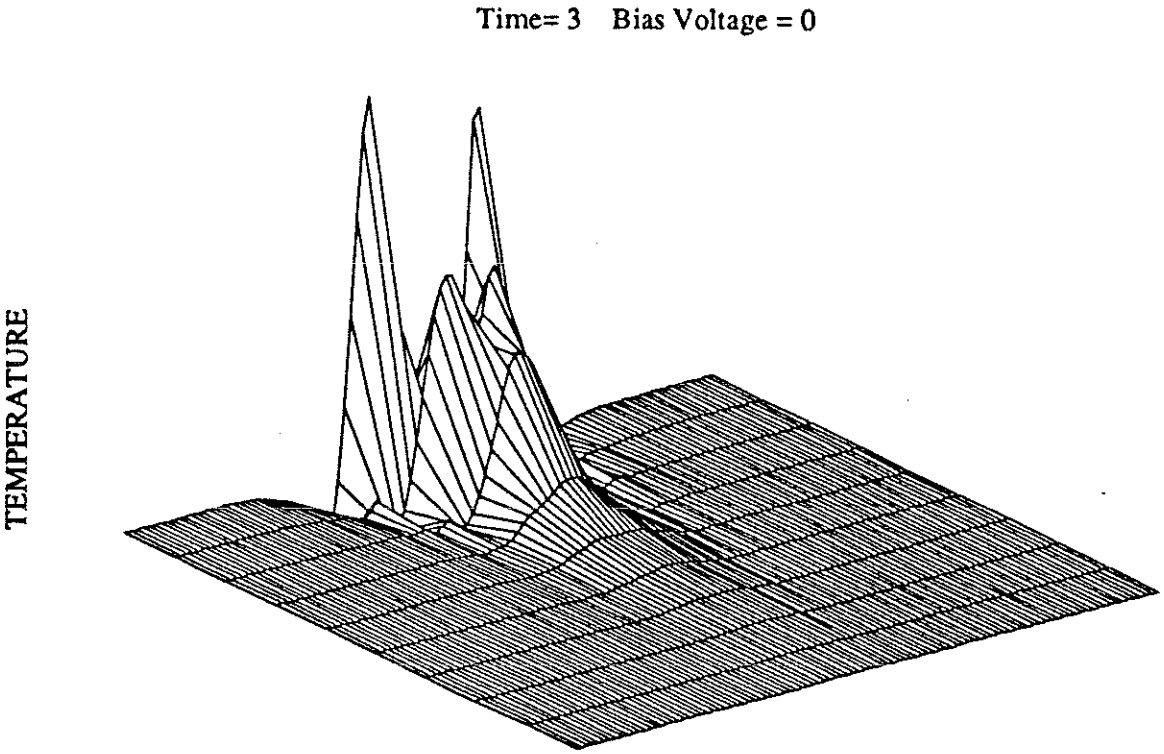

Fig 3: temperature

zero bias, $Time = 3$, $\frac{\Delta t}{\Delta x} = .2, \Delta x = .01$

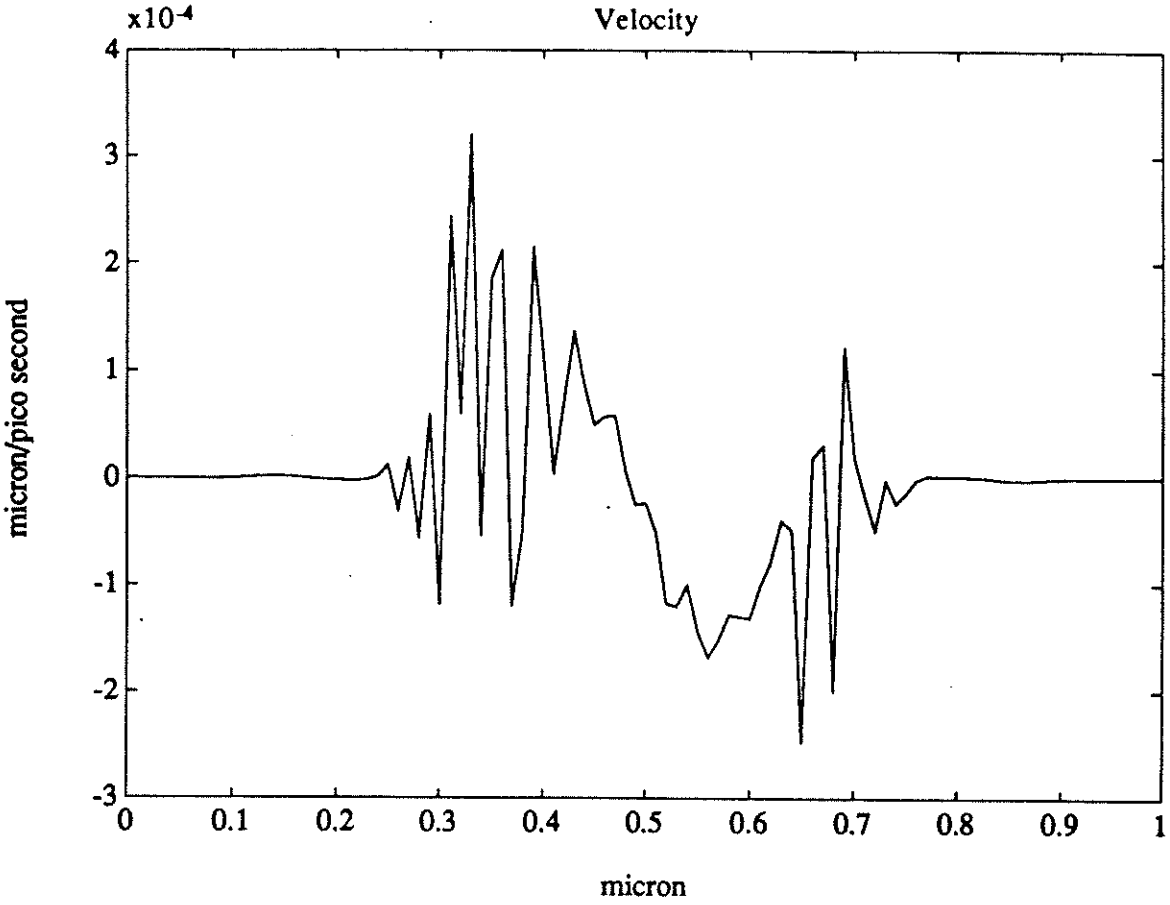

Fig 4: velocity in steady state

zero bias, $Time = 3$, $\frac{\Delta t}{\Delta x} = .2, \Delta x = .01$

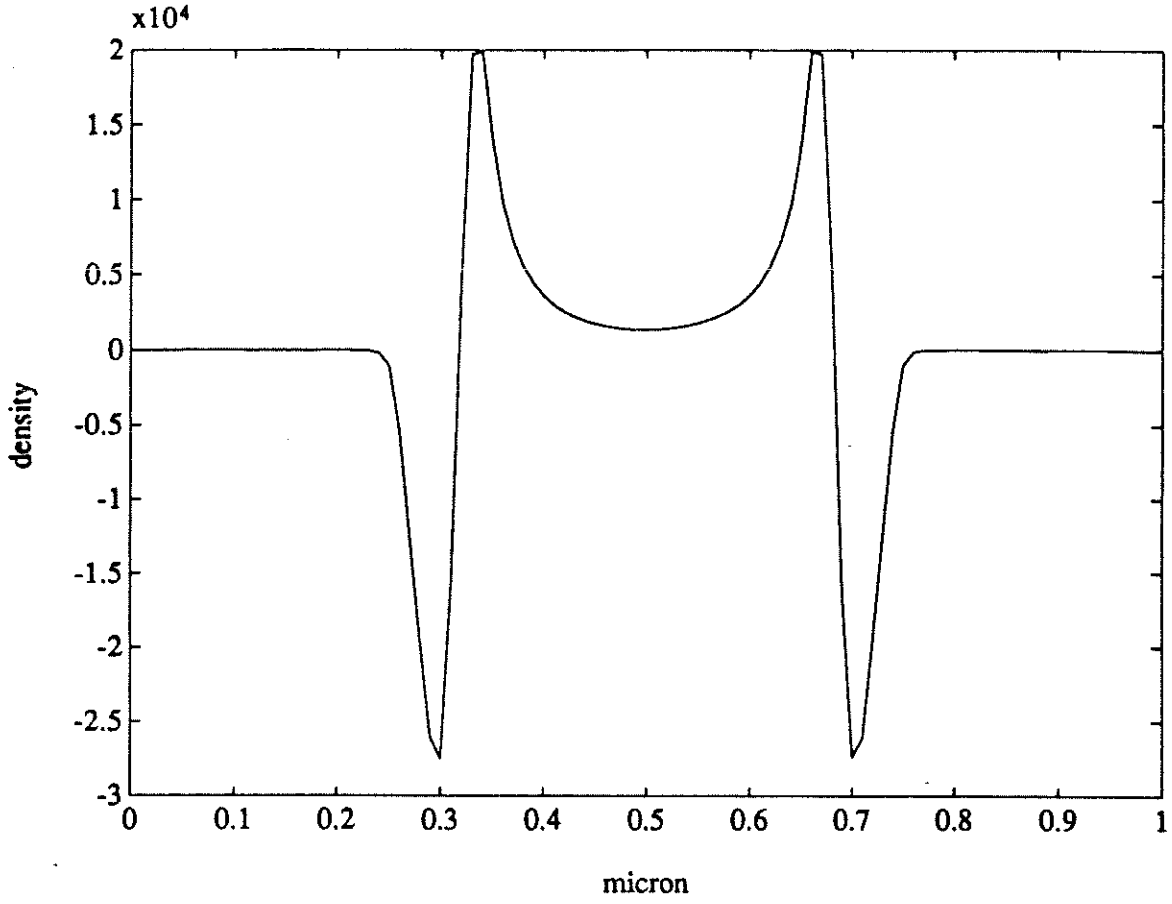

Fig 5: $n - n_D$ in steady state

zero bias, $T = 5, \frac{\Delta t}{\Delta x} = .2, \Delta x = .01$

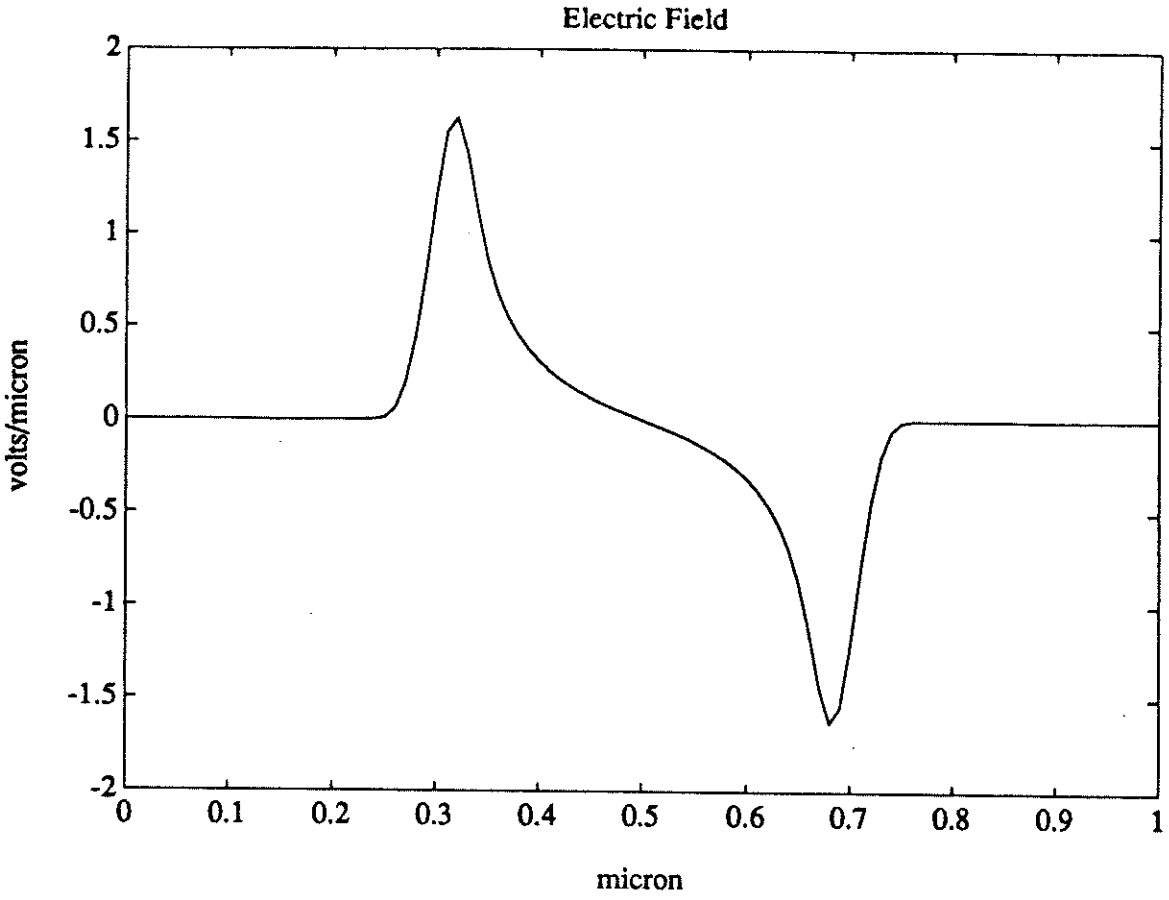

Fig 6: electric field in steady state

zero bias, $Time = 3, \frac{\Delta t}{\Delta x} = .2, \Delta x = .01$

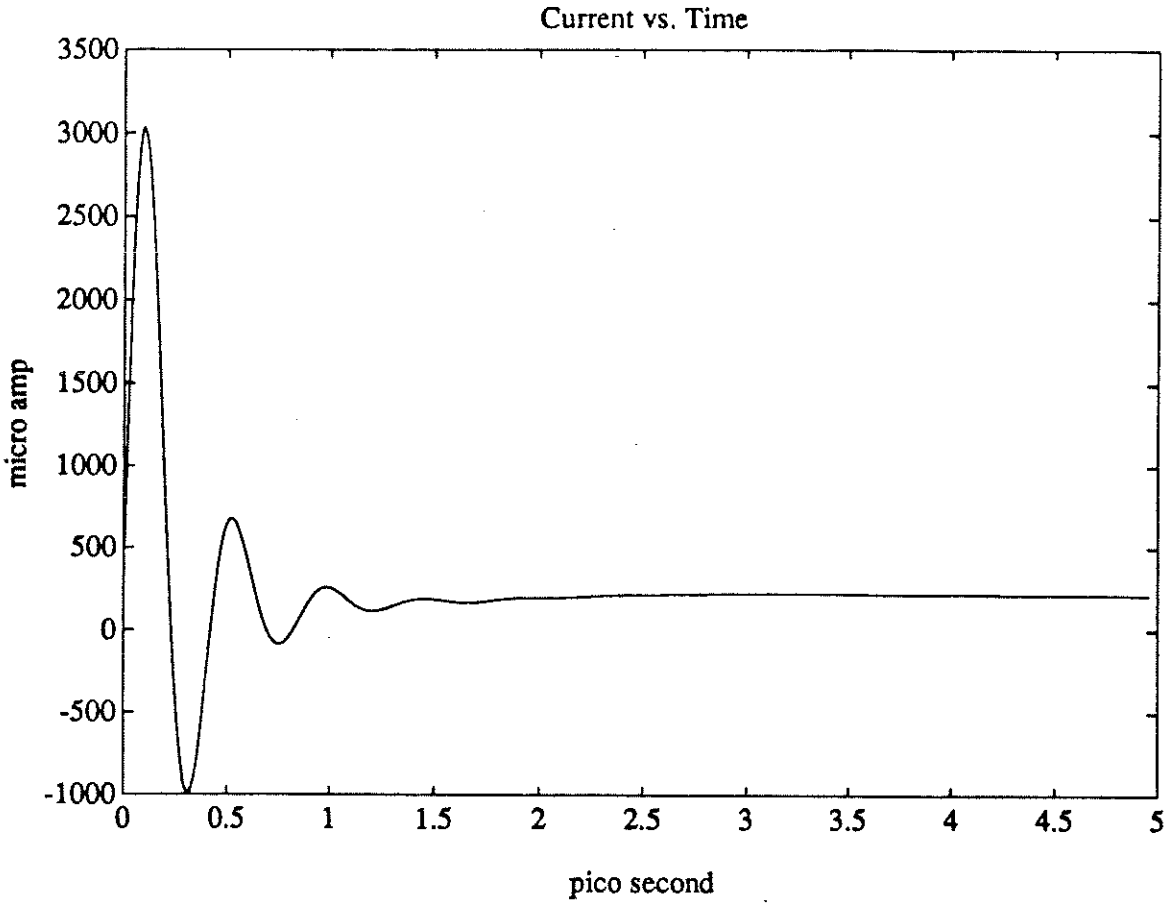

Fig 7: Current vs. Time

$v(t) = H(t),\ Time = 5, \frac{\Delta t}{\Delta x} = .2, \Delta x = .01$

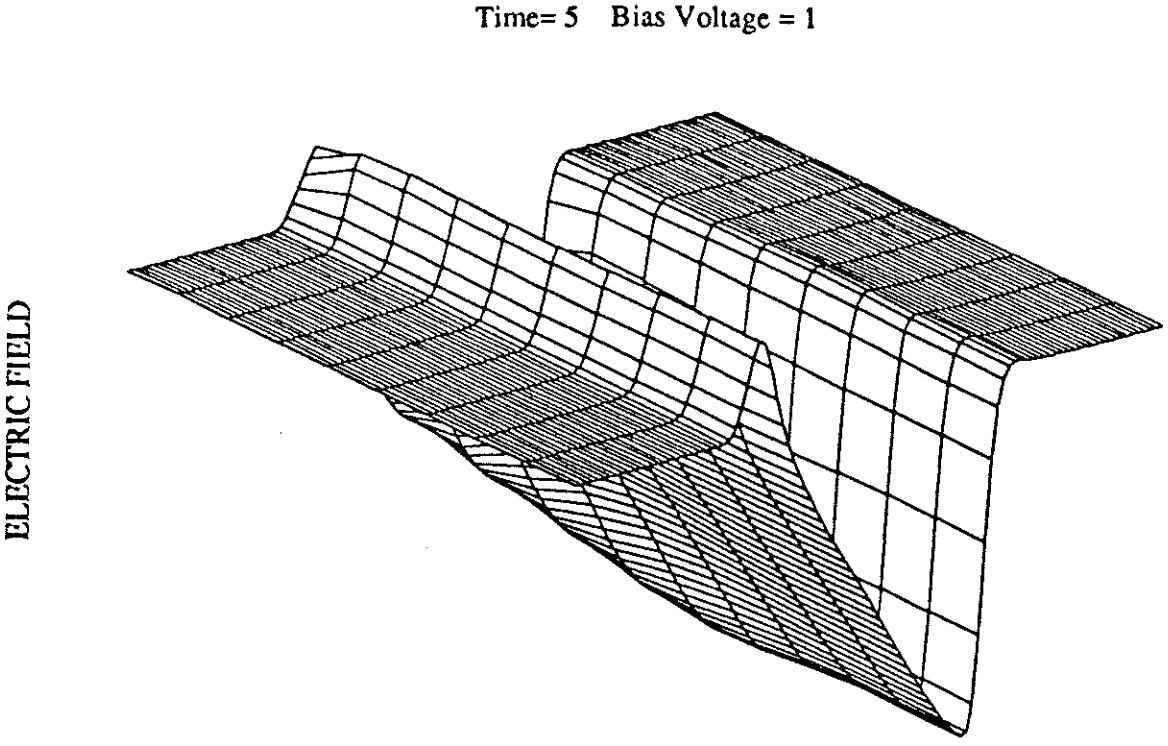

Fig 8: electric field in time

$v(t) = H(t),\ Time = 5, \frac{\Delta t}{\Delta x} = .2, \Delta x = .01$

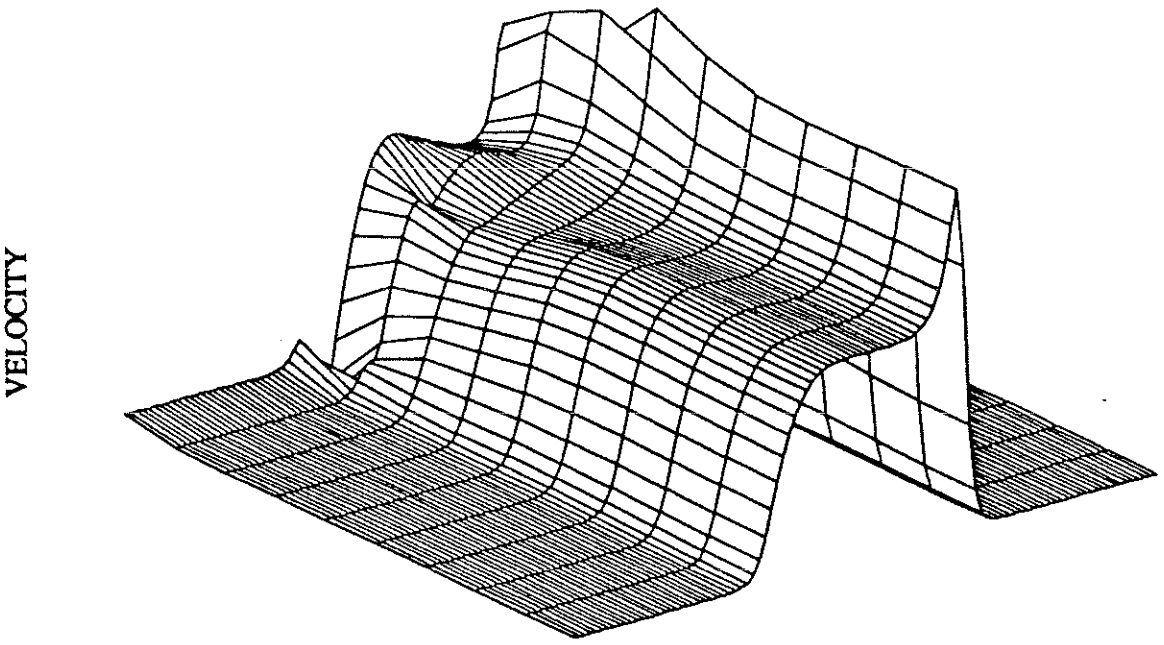

Fig 9: velocity in time

$v(t) = H(t),\ Time = 5, \frac{\Delta t}{\Delta x} = .2, \Delta x = .01$

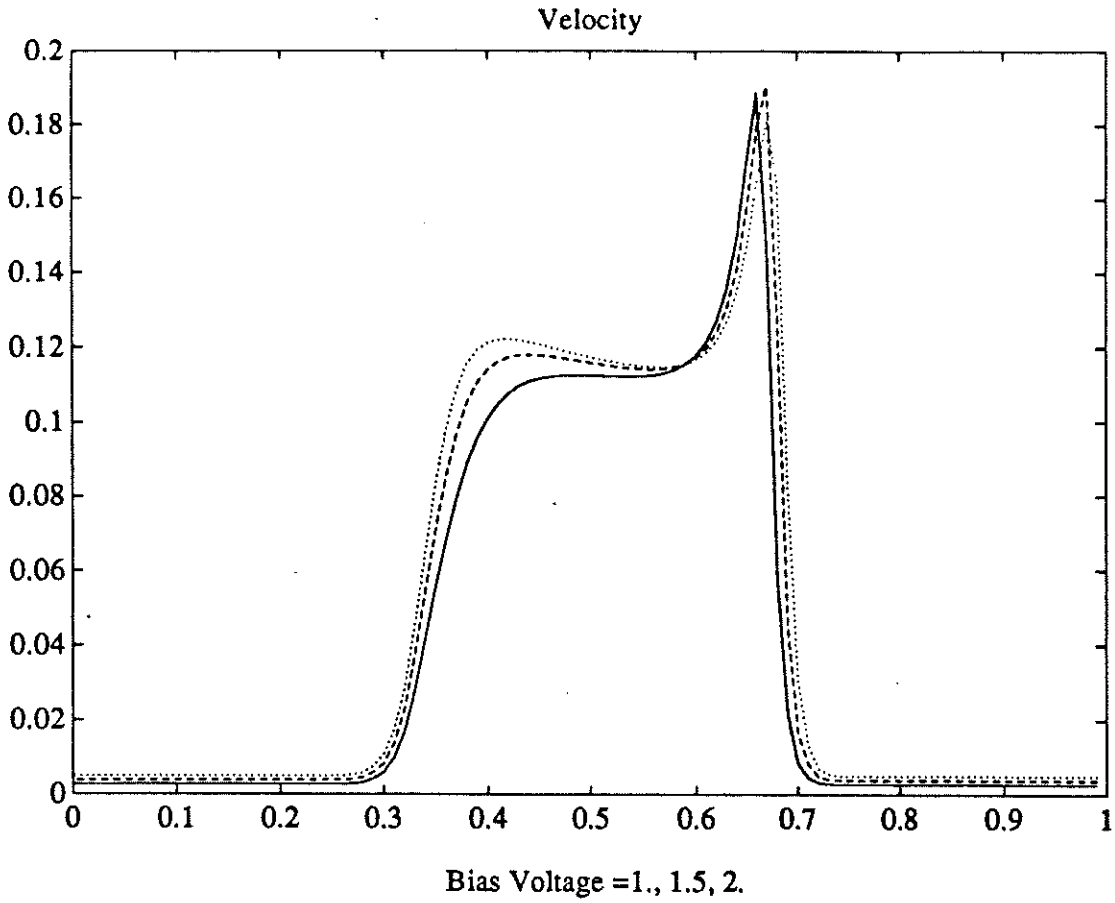

Fig 10: comparison of velocity profile for

bias voltage 1., 1.5, 2.

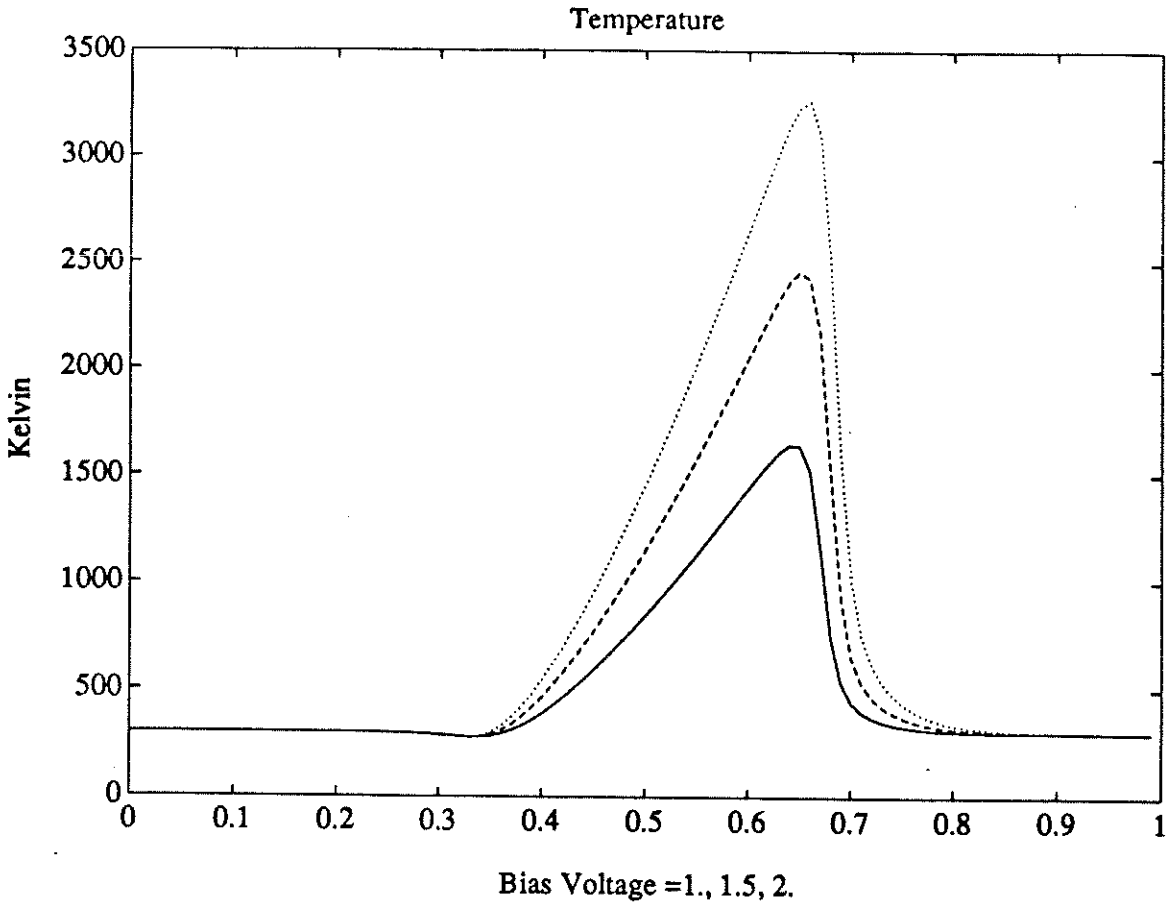

Fig 11: comparison of temperature profile for

bias voltage 1., 1.5, 2.

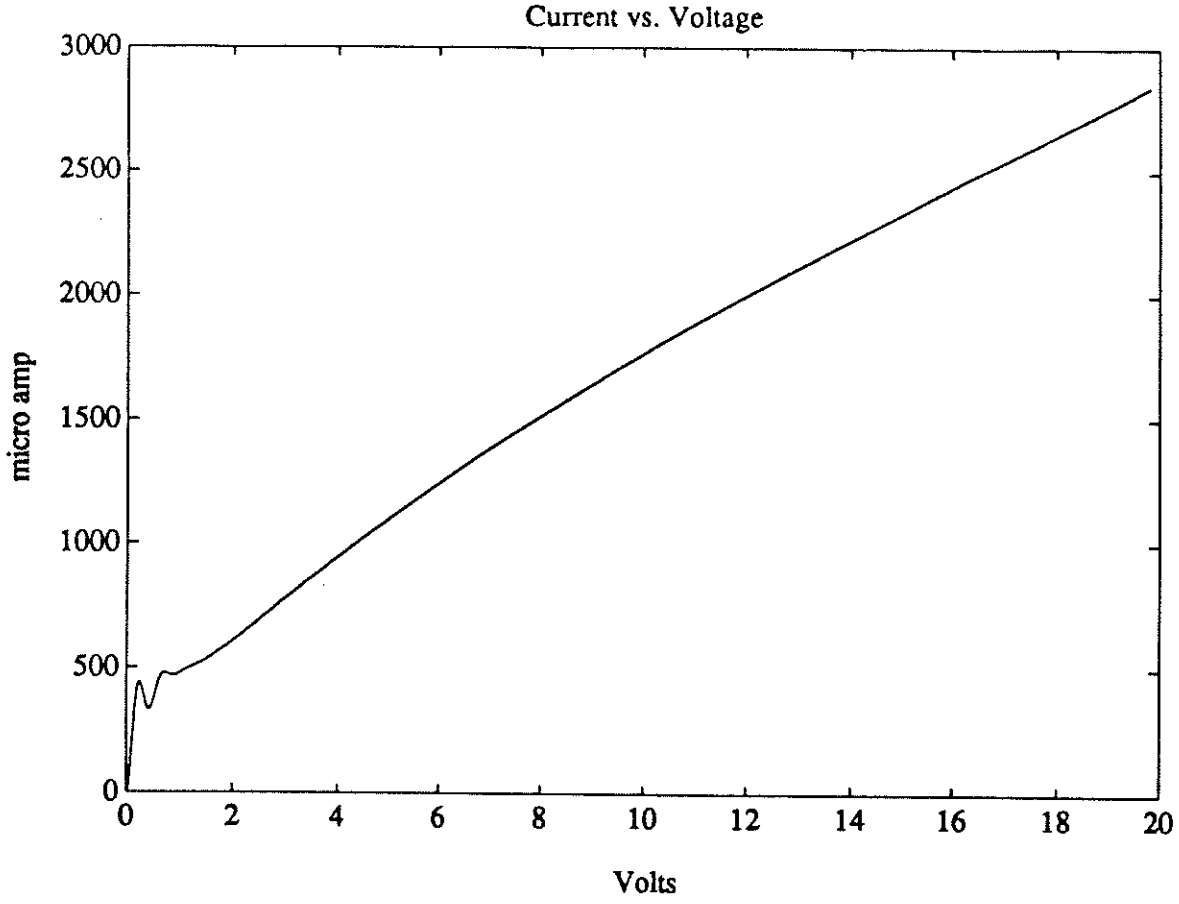

Fig 12: Current vs. Voltage

$v(t) = t,\ Time = 20, \frac{\Delta t}{\Delta x} = .1, \Delta x = .01$

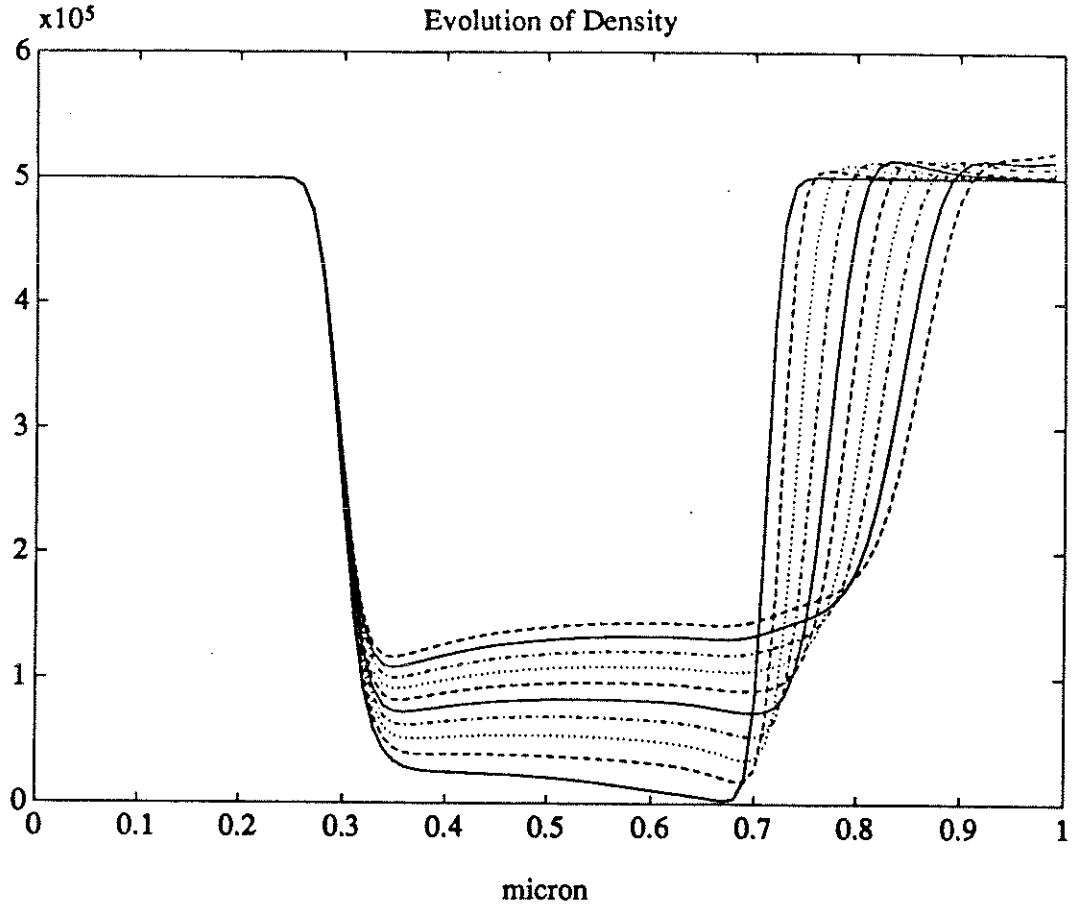

Fig 13: Evolution of density

$v(t) = t$, $Time = 20$, $\frac{\Delta t}{\Delta x} = .1, \Delta x = .01$

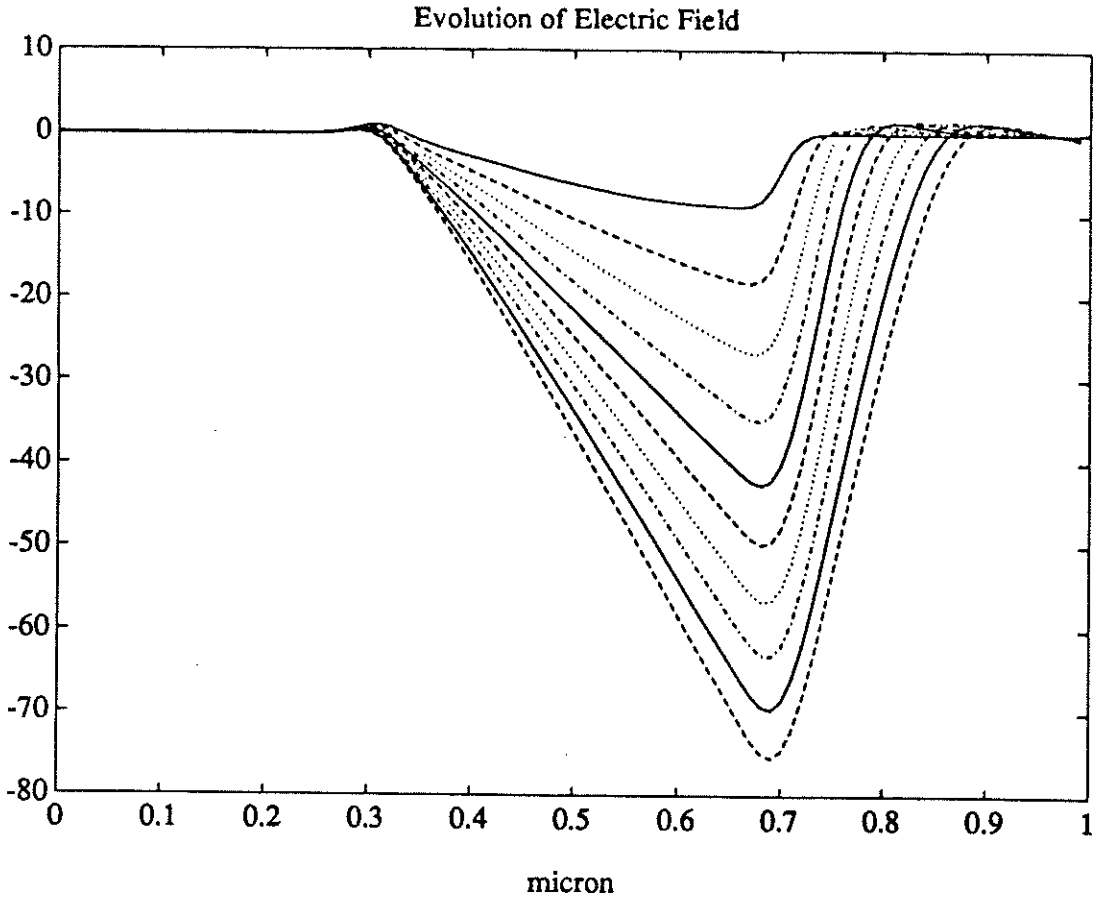

Fig 14: Evolution of electric field

$v(t) = t$, $Time = 20$, $\frac{\Delta t}{\Delta x} = .1, \Delta x = .01$

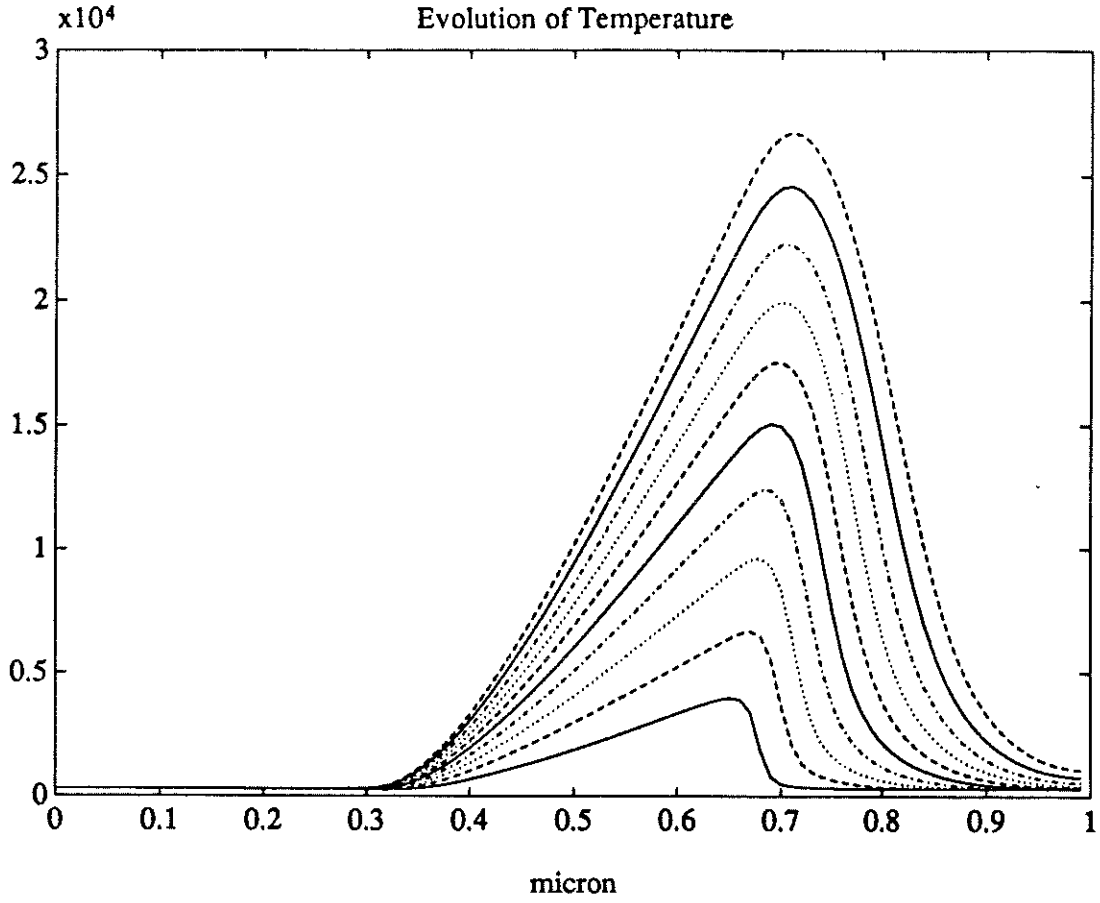

Fig 15: Evolution of temperature

$v(t) = t,\ Time = 20, \frac{\Delta t}{\Delta x} = .1, \Delta x = .01$

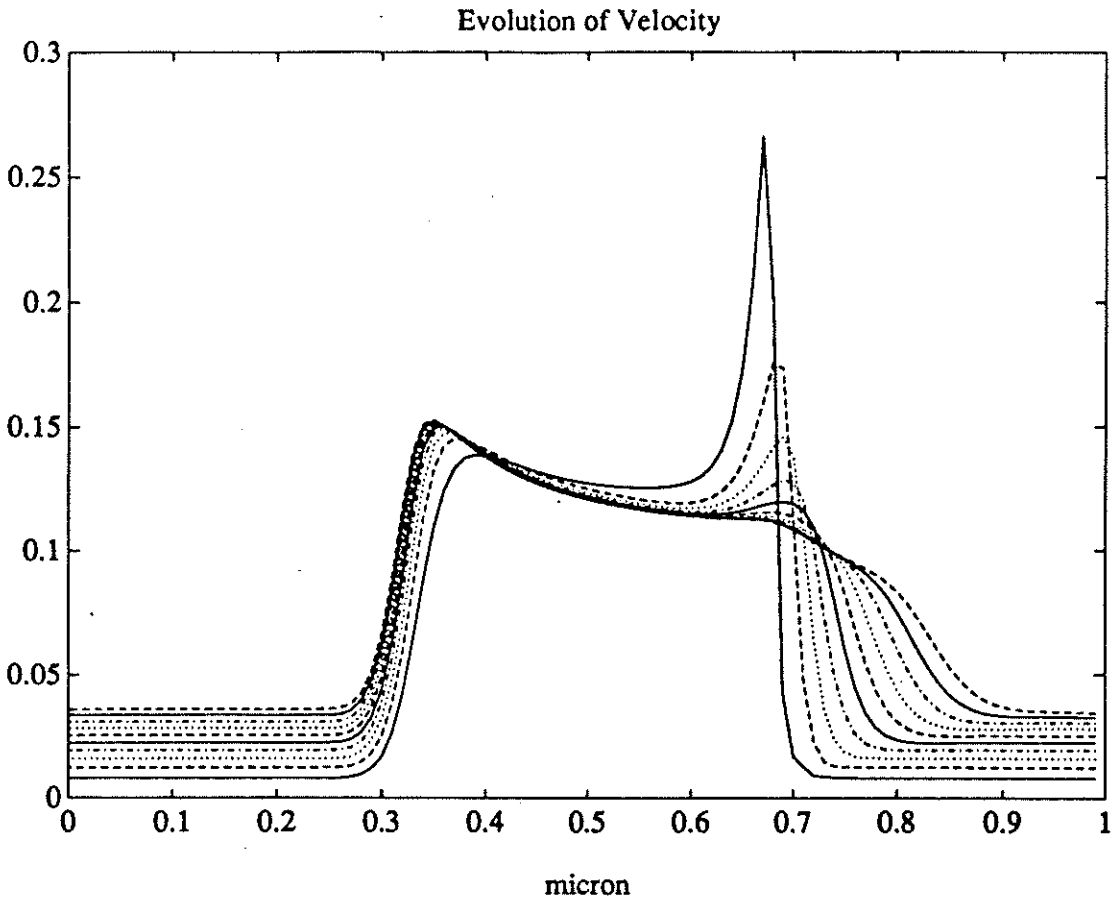

Fig 16: Evolution of velocity

$v(t) = t$, $Time = 20$, $\frac{\Delta t}{\Delta x} = .1, \Delta x = .01$

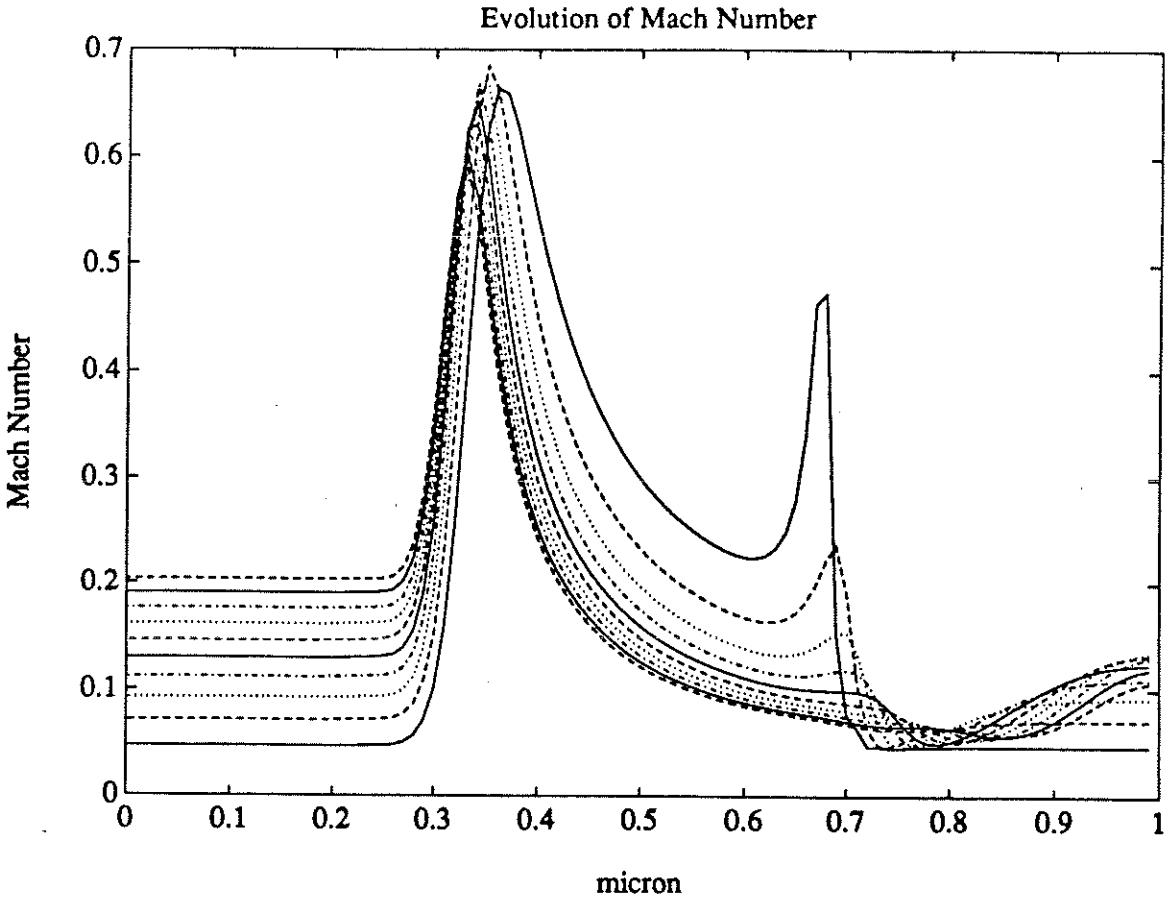

Fig 17: Evolution of Mach number

$v(t) = t,\ Time = 20,\ \frac{\Delta t}{\Delta x} = .1, \Delta x = .01$

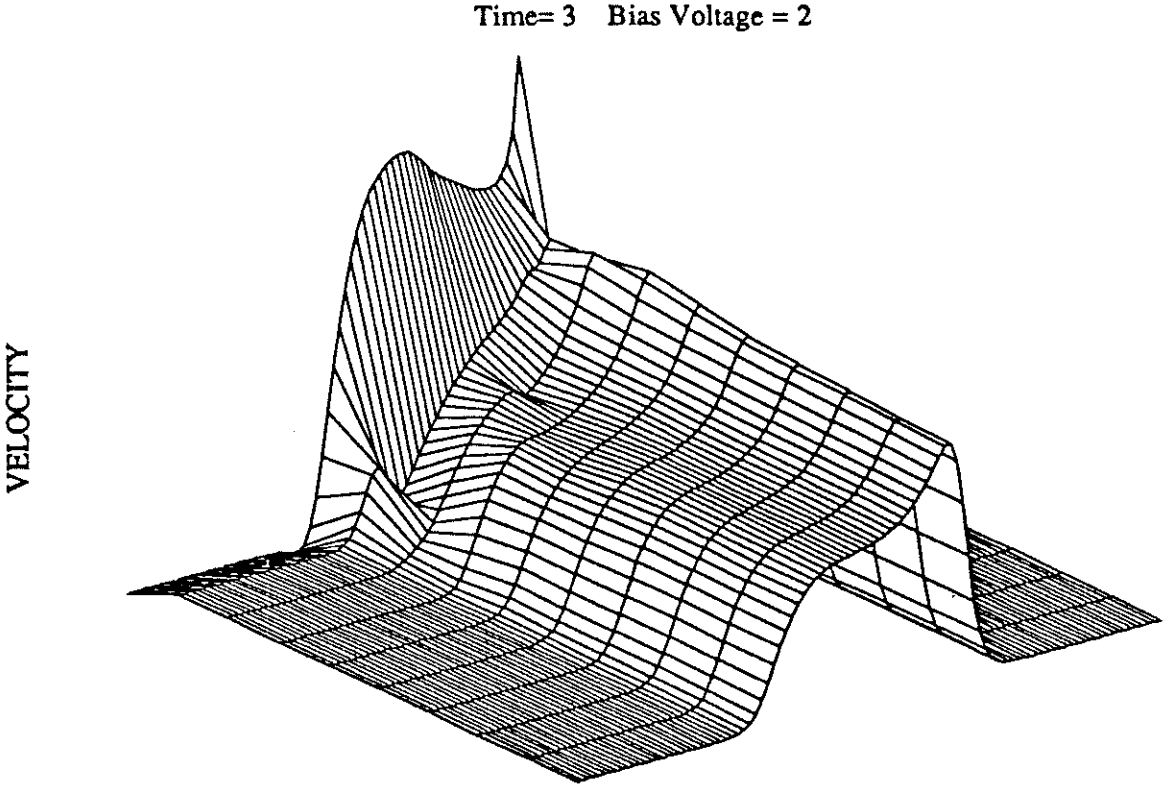

Fig 18: Velocity in time

$$v(t) = 2H(t),\ Time = 3, \frac{\Delta t}{\Delta x} = .1, \Delta x = .01, T_0 = 1000K$$

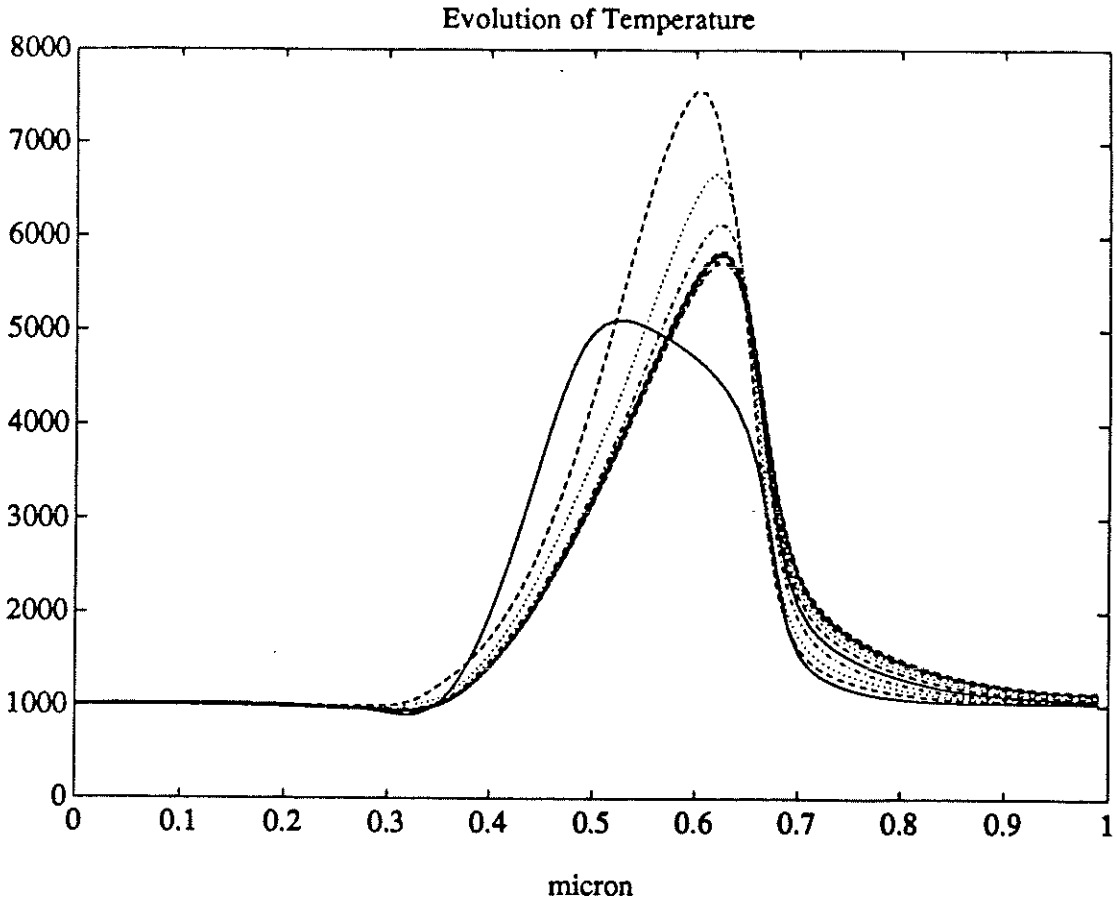

Fig 19: evolution of temperature

$v(t) = 2H(t),\ Time = 3, \frac{\Delta t}{\Delta x} = .1, \Delta x = .01, T_0 = 1000K$

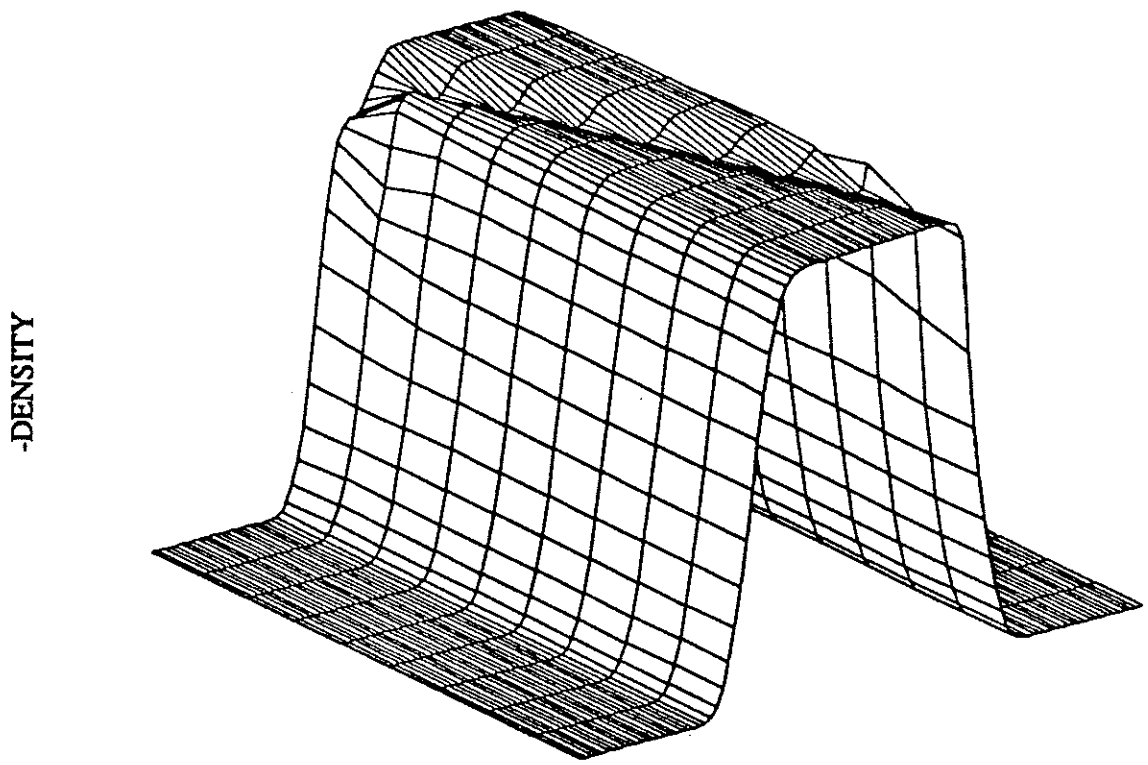

Fig 20: density in time

$v(t) = H(t),\ Time = 4, \frac{\Delta t}{\Delta x} = .01, \Delta x = .01, T_0 = 50K$

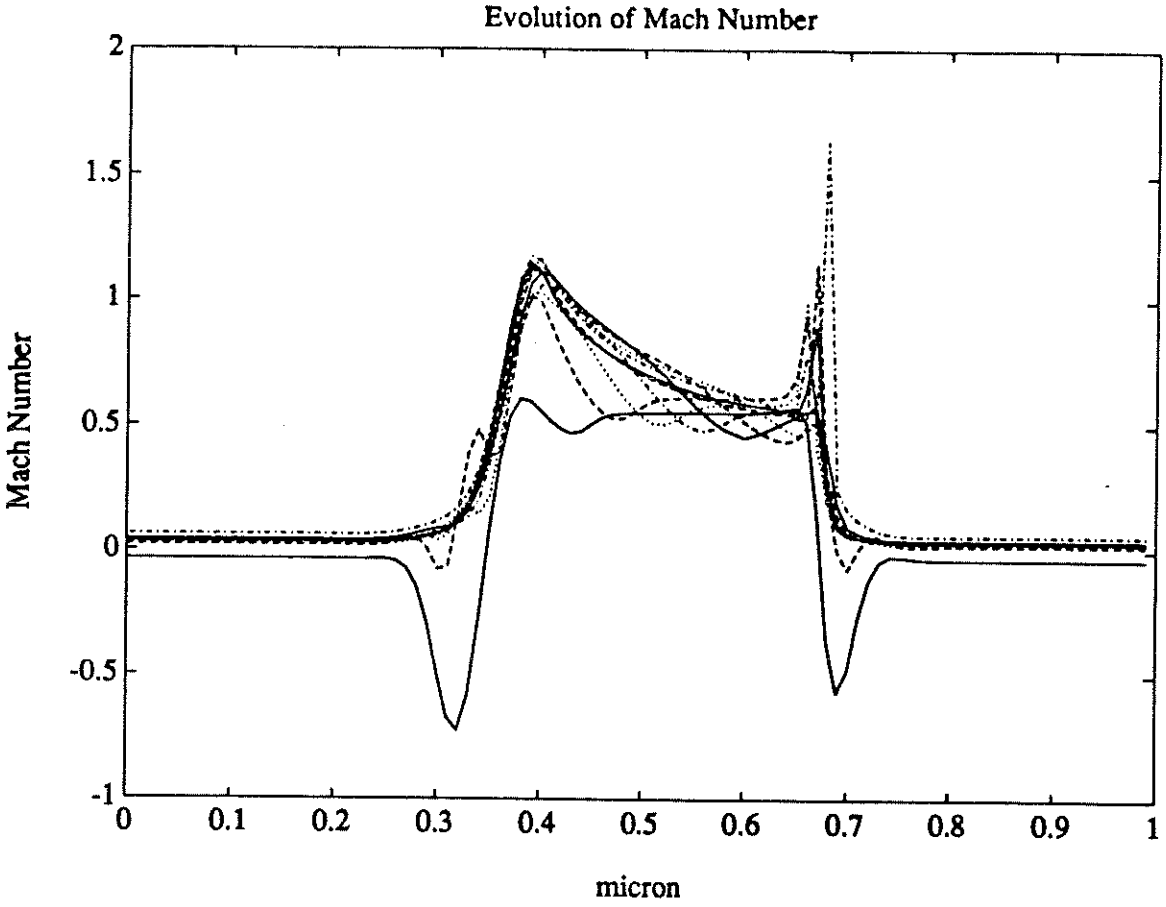

Fig 21: evolution of mach number

$v(t) = H(t),\ Time = 4, \frac{\Delta t}{\Delta x} = .01, \Delta x = .01, T_0 = 50K$

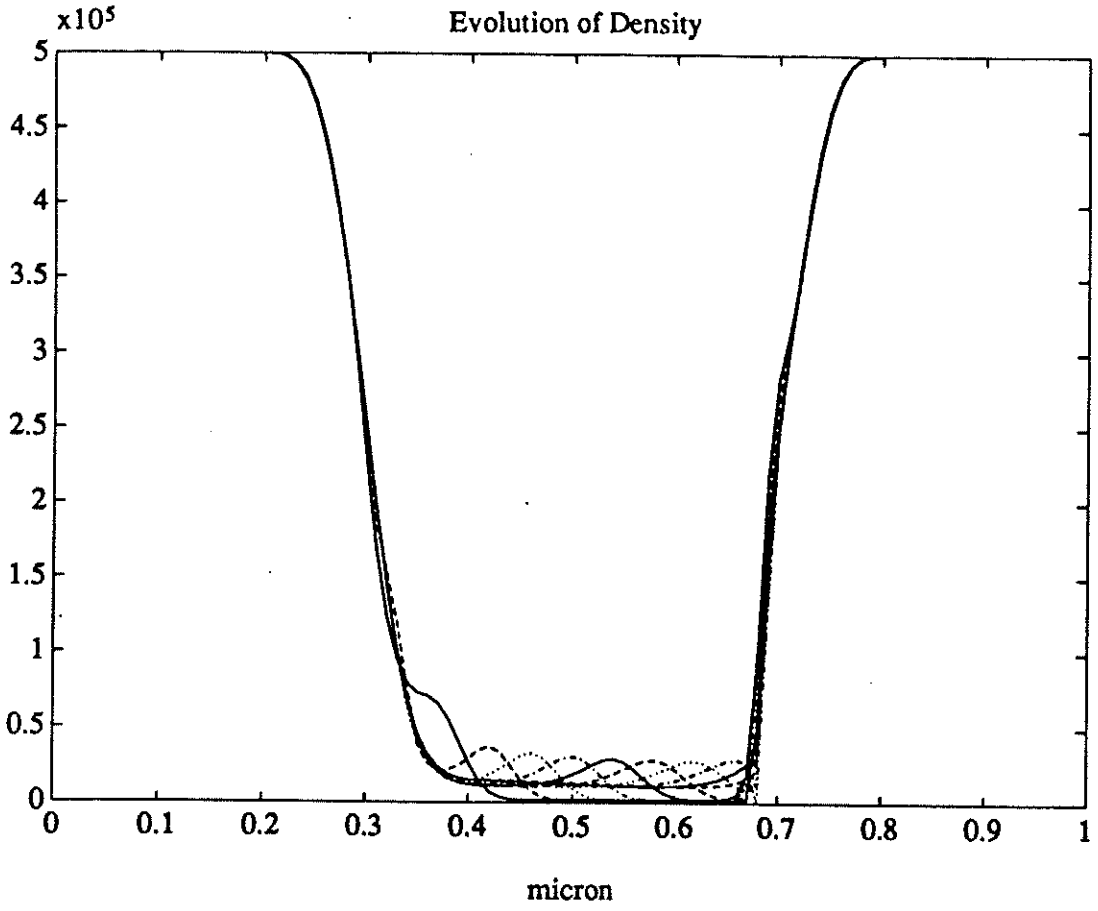

Fig 22: evolution of density

$v(t) = H(t),\ Time = 4, \frac{\Delta t}{\Delta x} = .01, \Delta x = .01, T_0 = 50K$

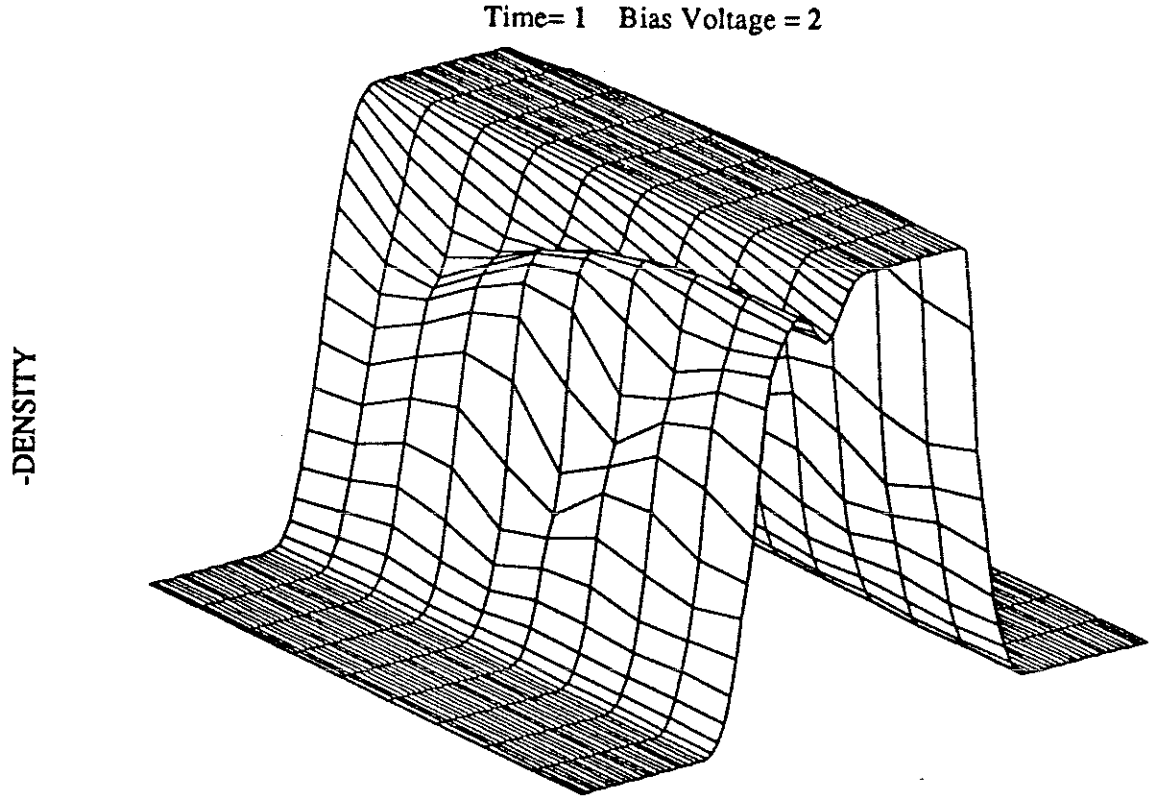

Fig 23: density in time

$v(t) = 2H(t),\ Time = 1, \frac{\Delta t}{\Delta x} = .01, \Delta x = .01, T_0 = 50K$

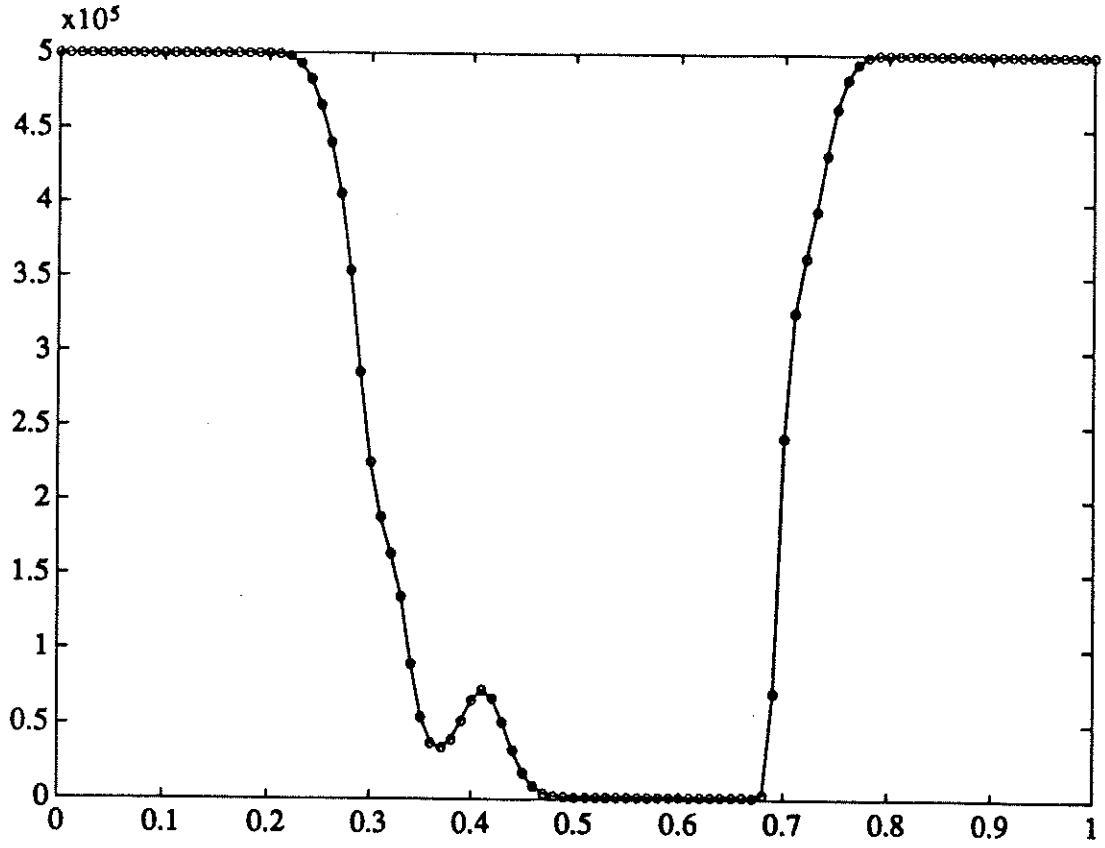

Fig 24: density

$v(t) = 2H(t),\ Time = 1, \frac{\Delta t}{\Delta x} = .01, \Delta x = .01, T_0 = 50K$

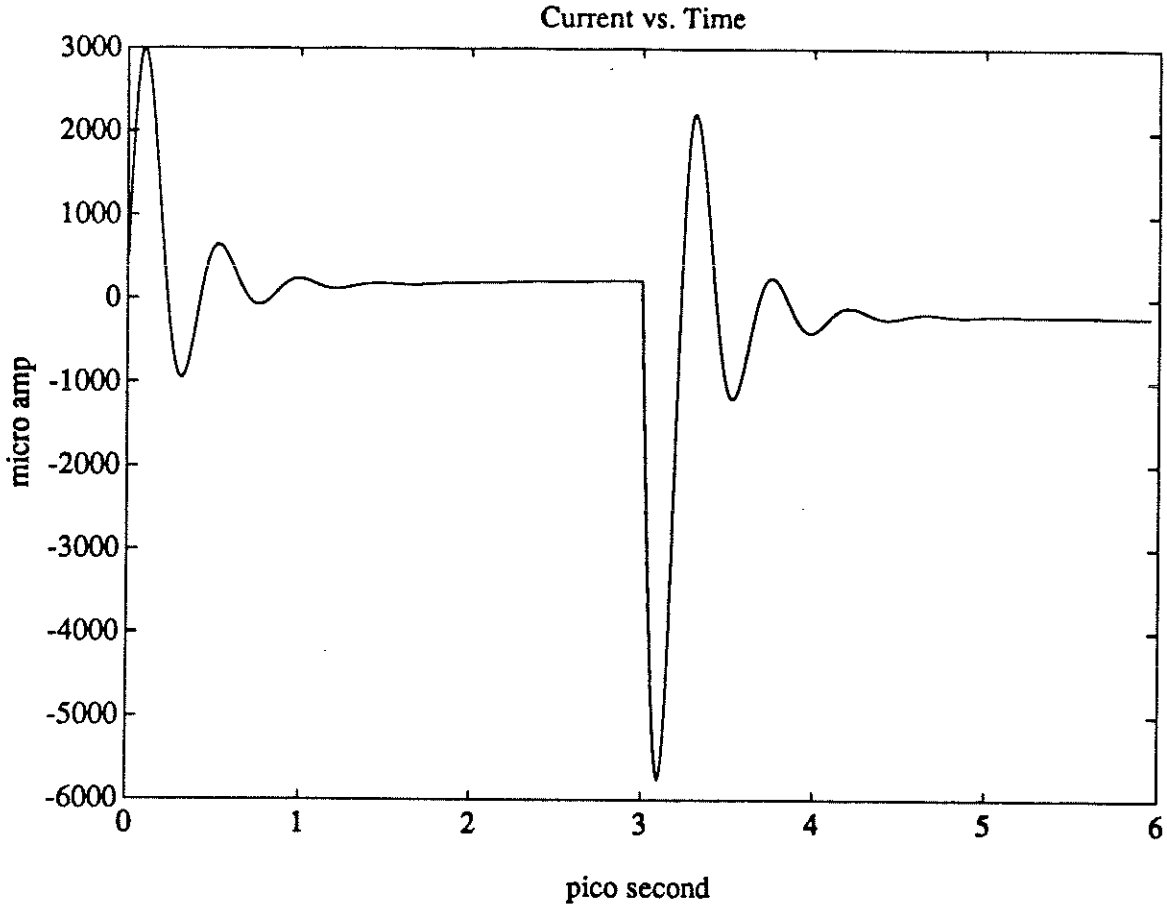

Fig 25: Current vs. Time

$v(t) = SQW(t),\ Time = 6, \frac{\Delta t}{\Delta x} = .1, \Delta x = .01, T_0 = 300K$

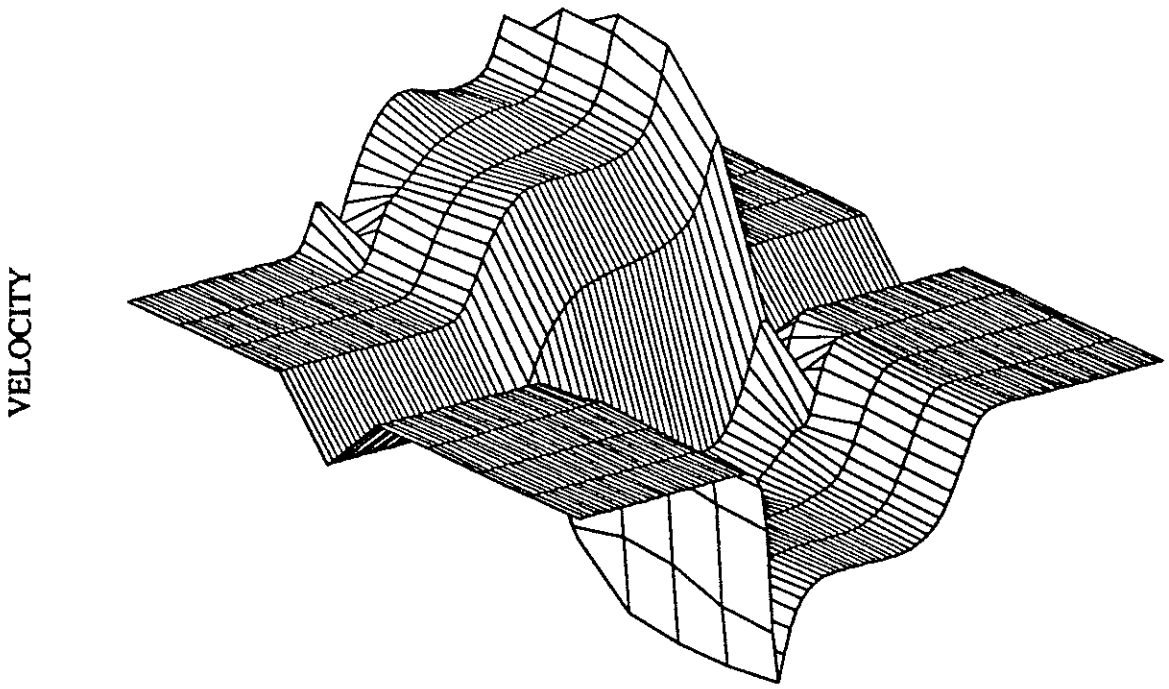

Fig 26: velocity in Time

$v(t) = SQW(t),\ Time = 6, \frac{\Delta t}{\Delta x} = .1, \Delta x = .01, T_0 = 300K$

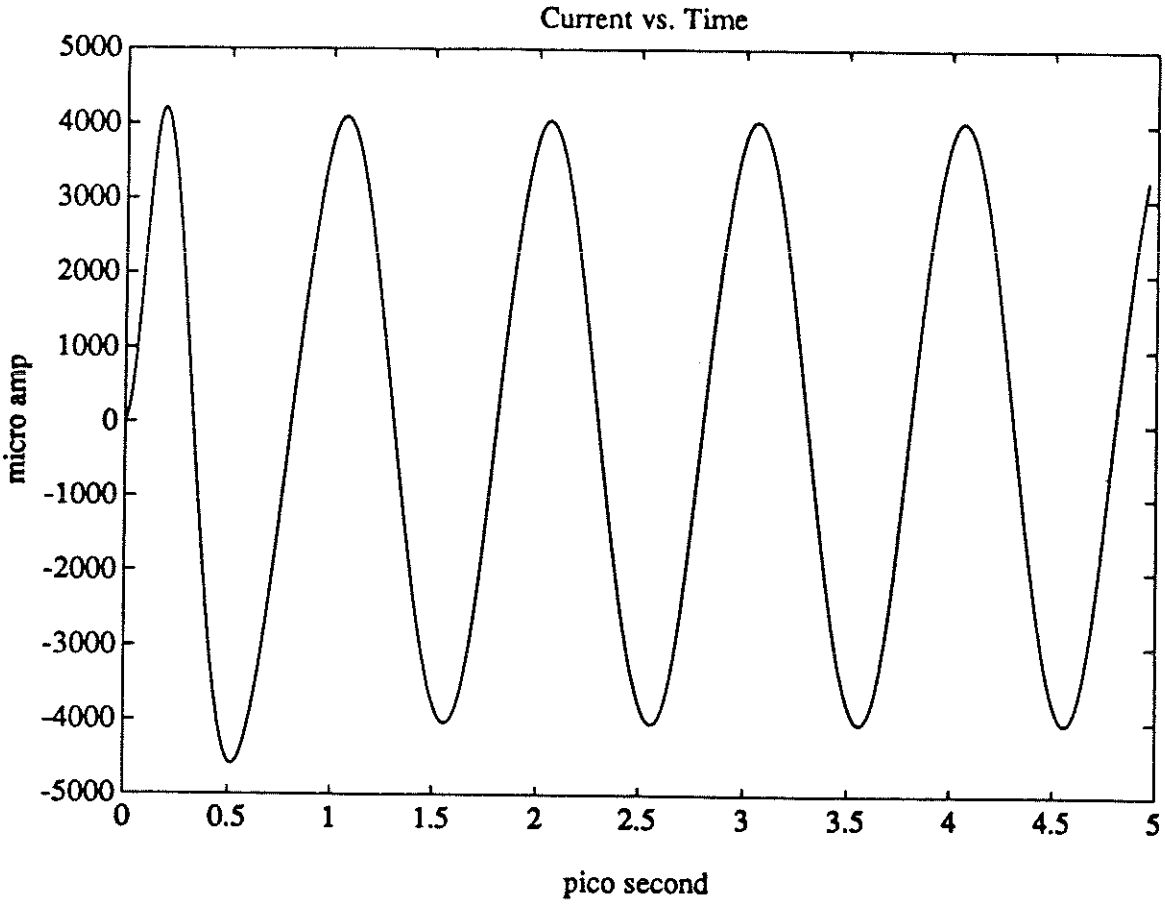

Fig 27: Current vs. Time

$v(t) = 2sin(2\pi t),\ Time = 6, \frac{\Delta t}{\Delta x} = .1, \Delta x = .01, T_0 = 300K$

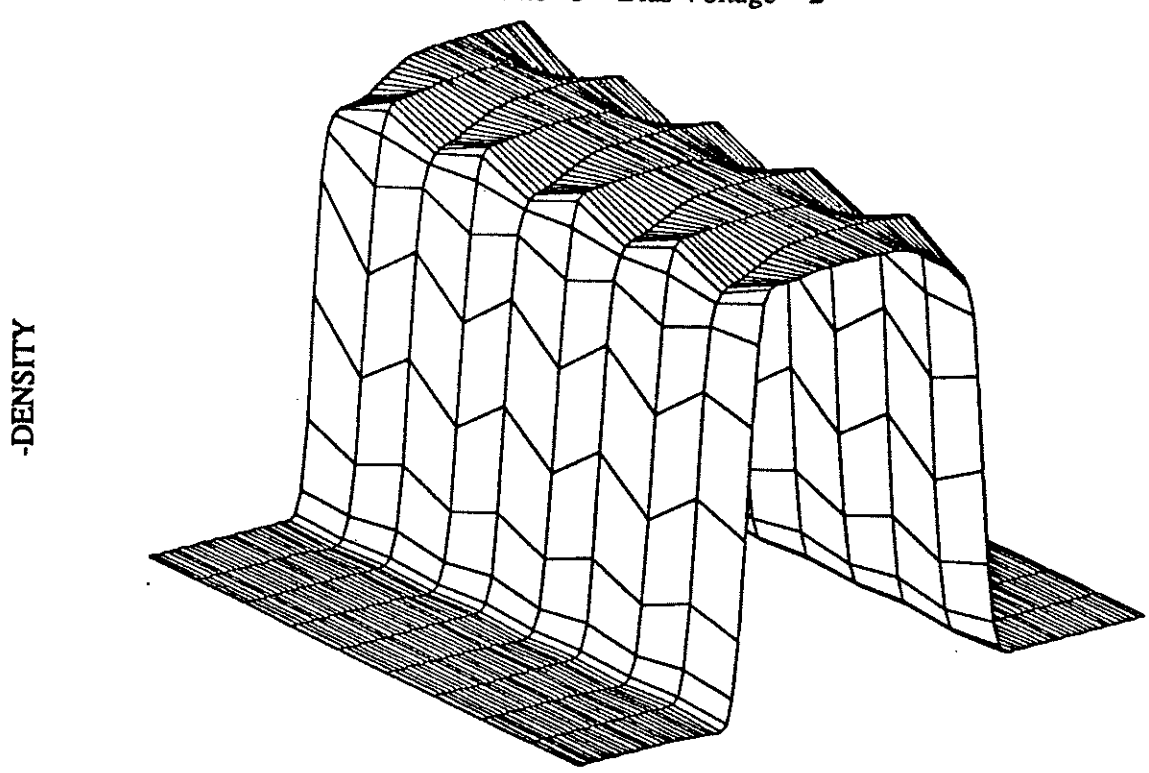

Fig 28: density in time

$v(t) = 2sin(2\pi t),\ Time = 5, \frac{\Delta t}{\Delta x} = .1, \Delta x = .01, T_0 = 300K$

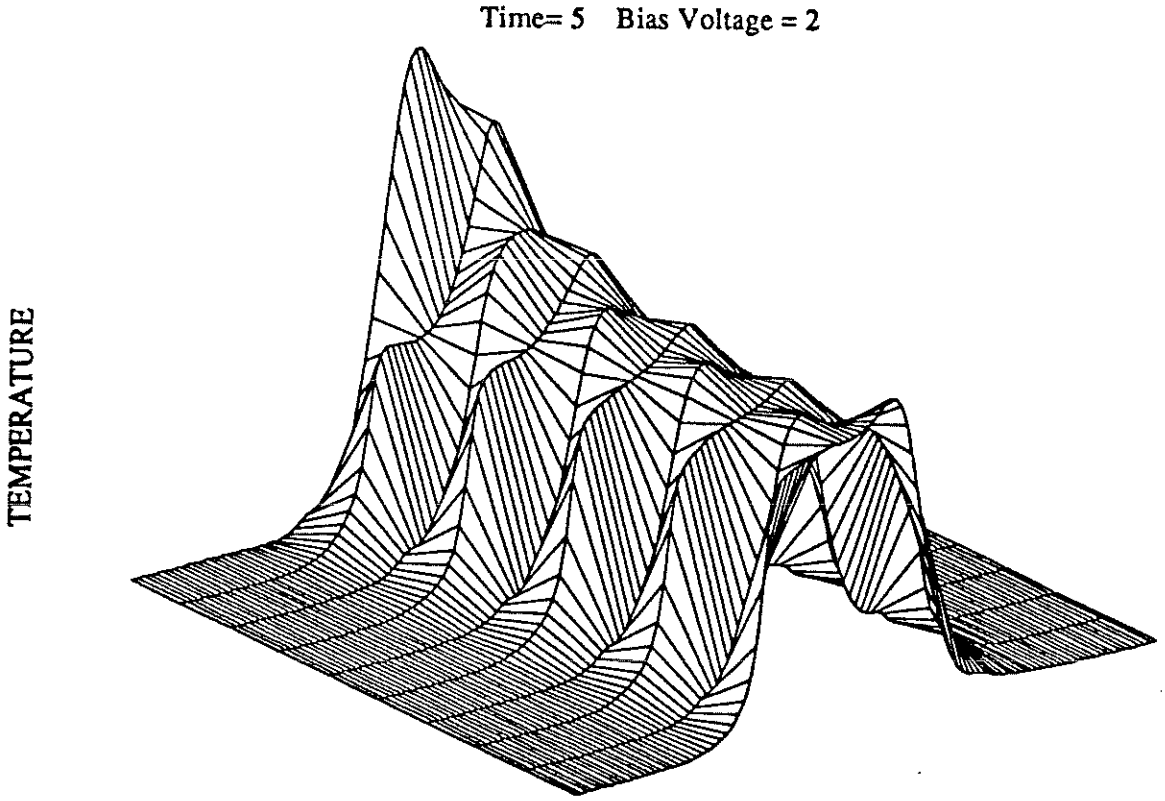

Fig 29: temperature in time

$$v(t) = 2sin(2\pi t),\ Time = 5, \frac{\Delta t}{\Delta x} = .1, \Delta x = .01, T_0 = 300K$$

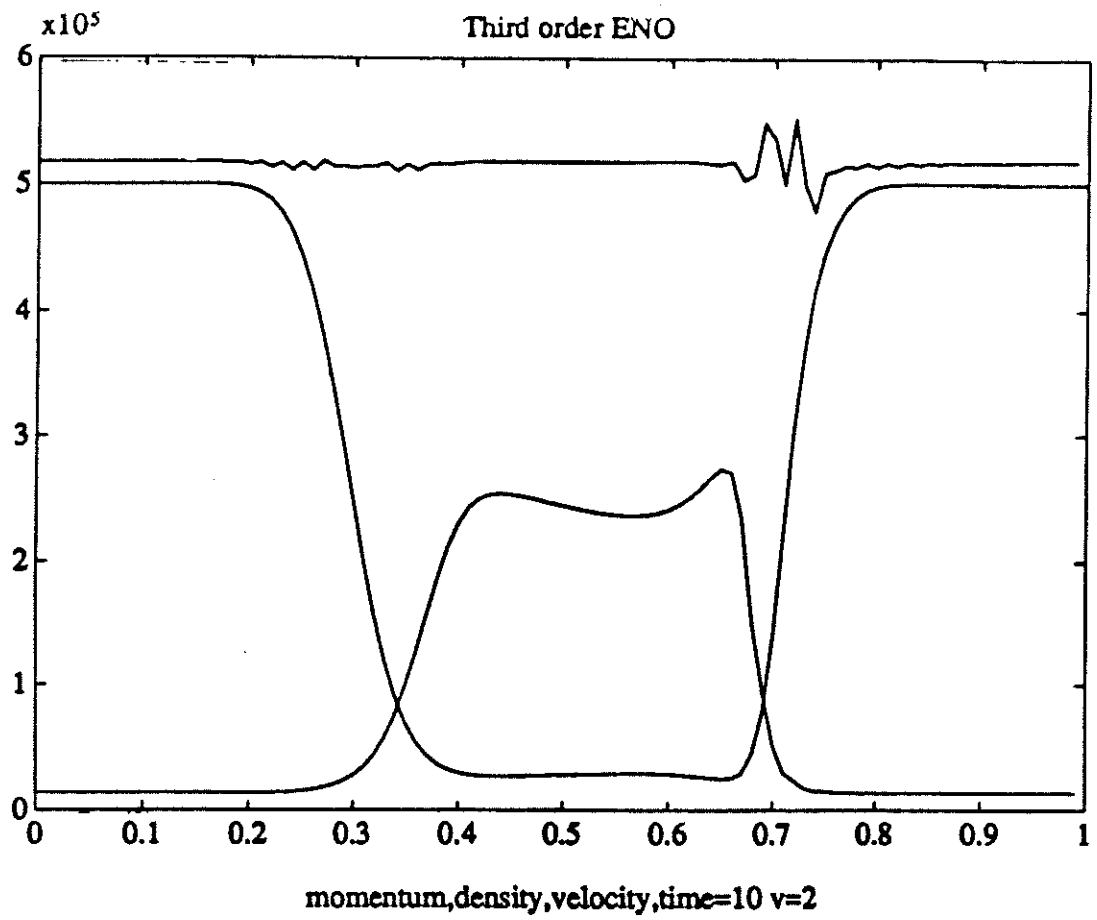

Fig 30: density, velocity, and momentum not to scale, third order stencil

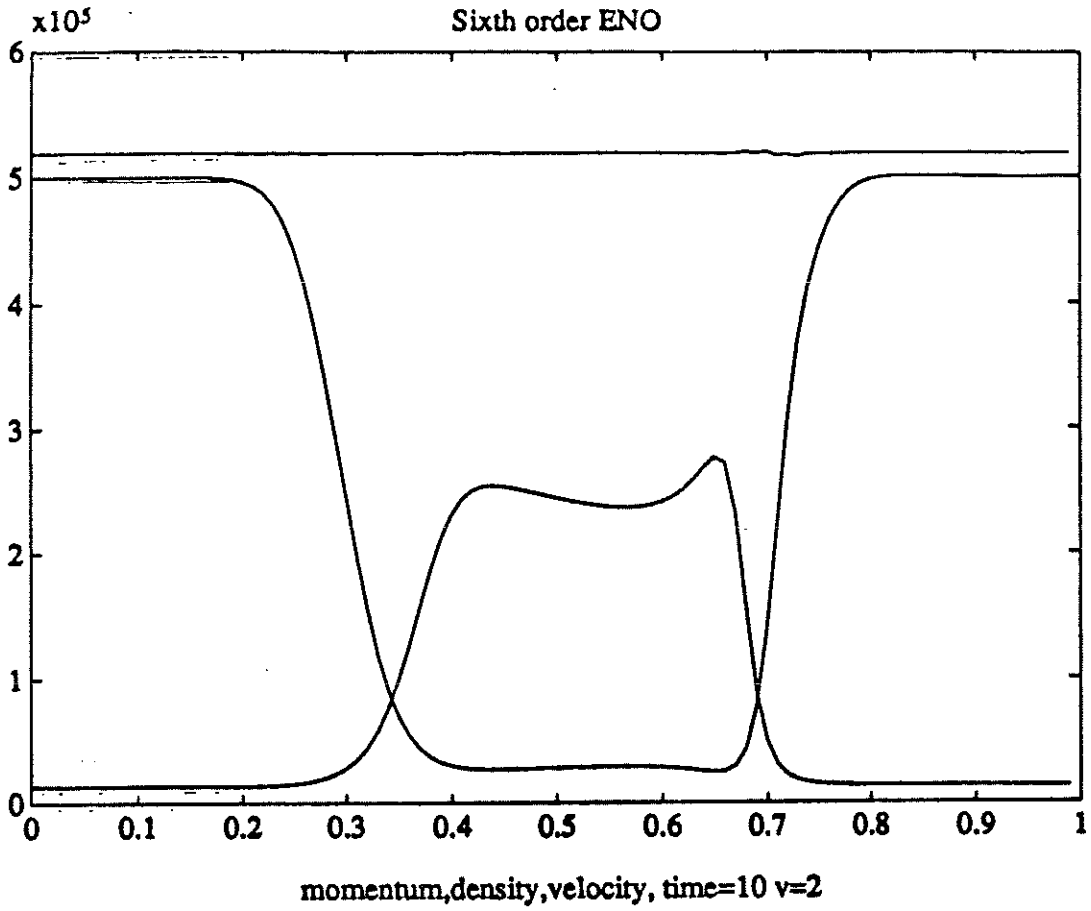

Fig 31: density, velocity, and momentum not to scale, sixth order stencil